CHARACTERIZATION OF SCHOTTKY BARRIER DIODES ON UNDOPED HYDROGENATED AMORPHOUS SILICON

A *Thesis Submitted*

in Partial fulfilment of the requirements

for the Degree of

Master of Technology

by

MD. NAZRUL ISLAM

to the

MATERIALS SCIENCE PROGRAMME

INDIAN INSTITUTE OF TECHNOLOGY KANPUR

MARCH, 1992

Dedicated to
my
all time friends

C E R T I F I C A T E

It is certified that the work contained in the thesis entitled "*Characterization of Schottky Barrier Diodes on Undoped Hydrogenaed Amorphous Silicon*", by *Md Nazrul Islam*, has been carried out under our supervision and that this work has not been submitted elsewhere for a degree.

Y. N. Mohapatra 30/3/92

Dr. Y. N. Mohapatra
Physiscs/Materials Science
I.I.T. Kanpur

Kumar 30/3/92

Dr. Satyendra Kumar
Physics
I.I.T. Kanpur

March, 1992

ACKNOWLEDGEMENTS

I am extremely grateful to Dr. Y. N. Mohapatra, Assistant Professor of Physics and Materials Science, Indian Institute of Technology, Kanpur, for his guidance and advice toward this thesis work. I am deeply indebted to him for his inspiration and invaluable contribution in introducing me to simulation and computational work.

To Dr. Satyendra Kumar, Assistant Professor, Department of Physics, Indian Institute of Technology, Kanpur, special thanks are due for his encouragement and dedicated contribution in my training in various aspects of experimental research. I also express a deep sense of gratitute to him for making this thesis work a success.

I would like to specially thank Dr. S. C. Agarwal, Professor in Physics Department, Indian Institute of Technology, Kanpur, for his advice, useful discussion and support for all programmes in his laboratory.

I also wish to thank Dr. K. Shahi, Assistant Professor, and Dr. K. N. Rai, Professor, Materials Science, Indian Institute of Technology, Kanpur, for allowing me to frequently use their laboratories.

Thanks are due to Ms. Pratima Agarwal, Mr. Anil Singh, Dr. Satyendra Kumar in enhancing my confidence as an experimentalist. I also acknowledge the encouragement and help I got from Ms. Shuily Gupta at Dr. K. N. Rai's lab., V. Padmanaban at Dr. K. Shahi's lab. in ACMS, and Mr. Sandeep Agarwal and Mr. L. S. Gupta at Solid State Devices lab., Western Block.

I also gratefully acknowledge the wholehearted cooperation rendered to me by all my lab. mates at both ACMS and Southern Block.

The assistance and encouragement I received, in many ways, from all my seniors and juniors in the Materials Science Programme is sincerely acknowledged.

I thank all the members and staff of ACMS for their cooperation and help. Liquid Nitrogen Plant and ACMS Workshop also need special mention. To Mr. B. K. Jain credits are due for some excellent figures in this thesis.

To my only class mate, Chacko Jacob, I have an opportunity to express a sense of thankfulness for making this course a success with his all round performance in assisting and encouraging me. I also owe a special dept to the trio of Swapan, Goutam and Sudhanshu for their help in my hour of need.

Many of my friends were responsible for making my stay at IIT Kanpur during this course a memorable one by providing me with their encouragement and moral support at the moment of distress. They are Manju Malhotra, Abdul Guffoor, Johnson John M., Subhash Chand, Premananda Bera, Srinivasa Rao, Nilesh Hiremath, Sudeepta Mukhapadhaya, Sudhakar, Gour Gopal Roy, Tapas Kumar Ray (TKda), P. G. Antony, Govind Kannan, T. K. Nath (Tapanda), Murlidharan, A. P. Prasad and many others.

I now realize the greatness of the efforts of a certain section of my school and college friends who helped me to reach this stage. They were specially Lovely Mishra, Ekbor Ali, Pritam Upadhyaya and Partha Kumar Biswas. I, therefore, feel appropriate to dedicate this thesis to them.

ABSTRACT

This thesis reports on the preparation of Schottky barrier on undoped hydrogenated amorphous silicon (a-Si:H) and its characterization using (i) Current-voltage (I-V) characteristics in the temperature range 269 K - 417 K, (ii) Internal photoemission (IPE) measurements and, (iii) Capacitance (C) and conductance (G) measurements as a function of both frequency and bias. From these measurements an attempt has been made to identify the predominant carrier transport mechanism and to extract Schottky diode parameters consistent with all measurements.

We have developed a simple simulation technique to model current-voltage relationship, which includes the effects of carrier recombination in the Schottky region, thermally assisted tunneling, and bulk series resistance (R_s). This technique helps in obtaining better and reliable values of barrier-height and more insight into carrier transport mechanism. Current-Voltage characteristics fit equally well to both diffusion and thermionic emission theory of carrier transport. However, on the basis of results obtained from simulation and internal photoemission, it is argued that the predominant mechanism is diffusion limited transport.

The main features of frequency as well as bias dependence of both capacitance and conductance are successfully explained using Gibb-Long model for ac response. The results obtained from dc and ac response measurements have been shown to be consistent.

LIST OF CONTENTS

LIST OF FIGURE CAPTIONS

Fig. 3.3. The forward-bias characteristics of dark I-V measured as a function of temperature.

Fig. 3.4. The reverse bias characteristics of dark I-V measured as a function of temperature.

Fig. 3.5. The extrapolated value of dark forward current (I) plotted in both thermionic emission theory (circles) and diffusion theory (stars).

Fig. 3.6. Logarithmic plot of bulk series resistance (R_s) estimated from high forward bias I-V data vs $10^3/T(K)$.

Fig. 3.7. A typical fit of the experimental room temperature I-V data (symbols) by simulation procedure (solid lines).

Fig. 3.8. A comparison of computer generated I-V curves (solid lines) with experimental forward bias I-V characteristics measured (symbols) as a function of temperature.

Fig. 3.9. The simulated value of saturation currents (I_s) plotted in both thermionic emission theory (circles) and diffusion theory (stars).

Fig. 3.10. The logarithm of simulated value of R_s plotted against the reciprocal of temperature (T).

Fig. 3.11. A schematic of the optical transitions that contribute to the photoresponse of a-Si:H Schottky diodes. (a) internal photoemission; (b) optical band-to-band transition; (C) localized to extended state absorption; and (D) absorption in the doped layer.

Fig. 3.12. Photoresponse of a-Si:H Schottky diodes under (a) forward bias and (b) reverse bias. [from Hich *et al*[32]]

Fig. 3.13. Fowler plot for the internal photoemission of electrons into intrinsic a-Si:H. [from Wronski *et al*[44]]

Fig. 3.14. Measured normalized photoresponse plotted with photon energy as a function of applied reverse bias across the Au/a-Si:H junction.

Fig. 3.15. Fowler plots as a function of reverse bias applied to the Au/a-Si:H Schottky barrier. Also shown its field dependence.

Fig. 3.16. Measured normalized photoresponse of Au/a-Si:H Schottky diode under (a) reverse bias 1 volt and (b) forward bias 1 volt.

Fig. 3.17. A Plot of ideality factor (n) as a function of temprature (T)

Fig. 4.1. Deep state trap release under (reverse) perturbing bias dV_s zero dc bias.

Fig. 4.2. Simplified theoretical variation of Schottky barrier differential capacitance with frequency: (a) for different temperatures; (b) for different interface potentials.

Fig. 4.3. Detailed models for capacitive response of the Schottky barrier: solid line ⇒ model of capacitance; dots ⇒ model of Viktorovitch and Moddel; dashes ⇒ approximation using equation (4.8) and the geometrical capacitance.

Fig. 4.4. Equivalent circuit (modeled by Gibb and Long) used in this work to model the sample behaviuor.

Fig. 4.5. Measured capacitance (C_m) and conductance (G_m) plotted as function of frequency at various applied dc bias voltages.

Fig. 4.6. Measured capacitance (C_m) versus dc bias applied to the Au/a-Si:H Schottky junction as a function of frequency. All C_m-V curves having maximum at ≈ 1.0 V.

Fig. 4.7. Corrected barrier capacitance (C_s) and conductance (G_s) versus frequency plot at zero dc bias.

Fig. 4.8. Influence of external dc bias voltage on corrected barrier capacitance versus frequency plots (both forward and reverse).

Fig. 4.9. Influence of external dc bias voltage on corrected barrier capacitance versus frequency plots (reverse bias).

CHAPTER I

INTRODUCTION

1.1 Introduction:

Semiconductors, as the name suggests, have very limited ability for electrical conduction. Their electrical properties are influenced and enhanced dramatically by supplying heat to them, exposing them to light or by the presence of extraneous materials in the host semiconductor. These unique properties of semiconductors become very useful when they form, in contact with other semiconductors or metals, rectifying junctions, which act as one-way valves to electrical current flow, current being allowed in one direction and limited in the other direction. Such a metal-semiconductor contact is known as a Schottky barrier after W. Schottky, who first proposed a model for barrier formation.

This rectifying nature of metallic contacts on copper, iron and lead sulfide crystals was discovered, more than a century ago, by Braun[1] in 1874. Since then numerous experimental and theoretical studies have been carried out, and are still going on. Initially Schottky contacts were used as point contact diodes, which employed a sharpened metallic wire in contact with an exposed semiconductor surface for radiowave detection in the early days of wireless technology. It was the Second World War, where it was used in microwave radar, which brought a revolution in the

understanding of the physics of Schottky barriers. Point contact rectifiers proved highly unreliable in their characteristics and were subsequently replaced by deposition of a thin metallic film on a properly prepared surface of semiconductor. These contacts have shown much superior characteristics and hence widened the field in its research and development. These activities were inspired to a considerable extent because of the importance of metallic contacts in semiconductor technology. As a result of this development, further areas of application of Schottky barriers (as photodiodes, photovoltaic devices, light emitting diodes, metal-semiconductor field effective transistors etc.) have emerged. Thus Schottky barriers are now being used on a large scale in various fields of semiconductor device technologies.

1.2 Amorphous Semiconductors :

Apart from these above mentioned applications in the world of crystalline semiconductors, Schottky barriers have more recently, drawn special attention with the discovery of amorphous semiconductors, which are disordered, in the absence of long-range periodic structure. These materials can be prepared in thin film form and are relatively inexpensive. Amorphous thin films have high coefficients for light absorption and are unaffected by high energy radiations because of their unique property of disorderedness. Therefore, these materials are of great importance

from technological point of view. Although disorderedness endows amorphous materials with the above advantages, disorderedness itself creates hurdles in the way of their application by inducing localized electronic states well within the forbidden energy region. The localized states do not contribute to electrical conduction in normal case[2], as the mobility of these electrons are negligible compared to that of conduction electrons. These disorder-induced electronic states are intrinsic to amorphous semiconductors, and have continuous energy spectrum as compared to extrinsic and discrete localized states, associated with impurity atoms within the host crystalline semiconductors energy gap. Because of these continuous distribution of states in the gap, and the deviation in the bond angles and bond lengths, valence and conduction bands in amorphous semiconductors have got tails extended into the forbidden region. Fig. 1.1a shows a typical energy band diagram for amorphous semiconductors. The hatched region are of localized states while the unhatched regions are of delocalised or extended states, where electrons are free to move with finite mobility. Because of band tails it is difficult to define the band edges. But Fig. 1.1b clearly shows that the carrier mobility is negligible within the localized regions and increases sharply at a certain energy ($E_{\mu v}$ or $E_{\mu c}$). The states for which carrier mobility is finite are called extended states. Therefore, we can see a well defined demarcation line, in terms of

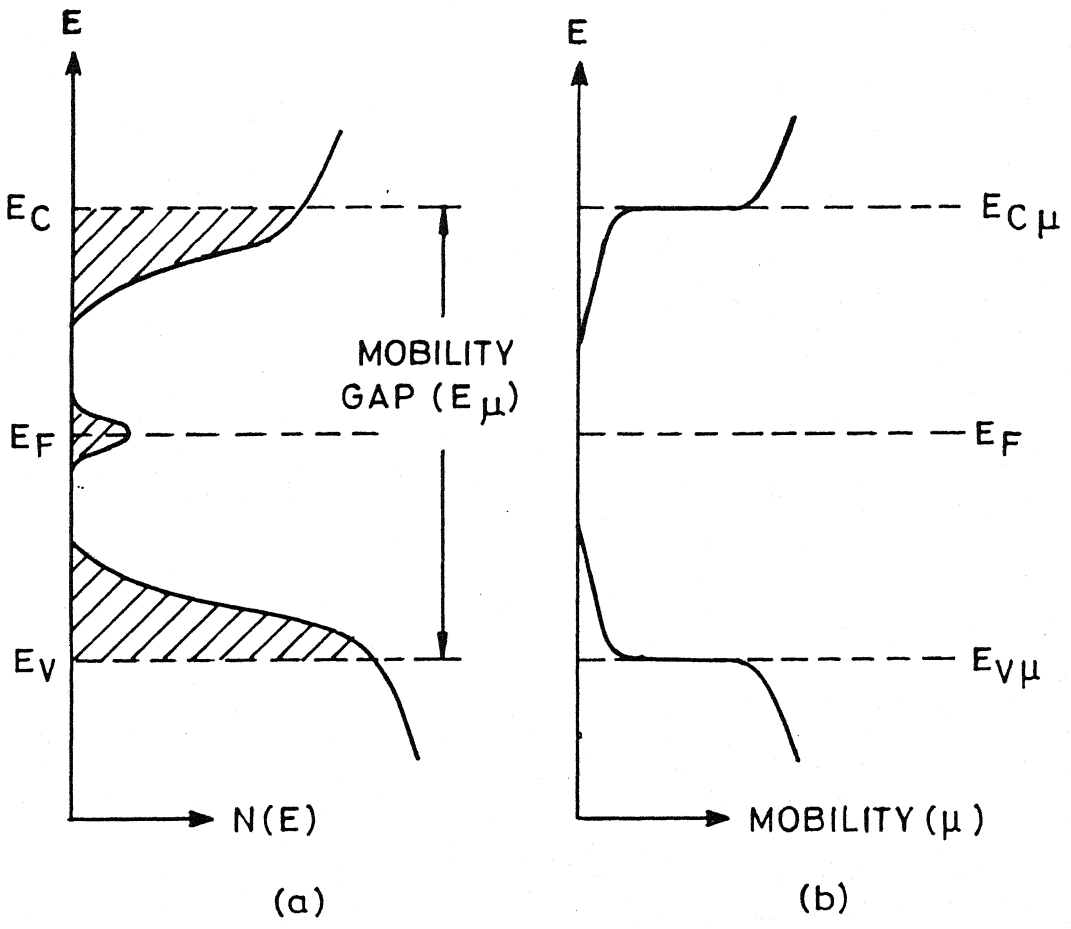

Fig. 1.1. A typical energy band diagram for amorphous silicon: (a) real gap in the density of states (DOS) and a finite DOS at E_F; (b) negligible carrier mobility in the forbidden energy region. [from Devis and Mott[2]]

mobility, between extended and localized states. These are called mobility edges and the energy difference between the mobility edges is known as mobility gap, which resembles semiconductor band gap in crystalline semiconductors. The properties of amorphous semiconductors are greatly dominated and controlled by the shape of the band tails and densities of localized states (DOS) in the gap. Numerous research and developmental work has been attempted to control DOS and its distribution in the gap. It has been observed that the presence of hydrogen atoms (~3 at.% to as much as 50 at.%) in the amorphous silicon reduces DOS and hence improves its electrical and optical characteristics remarkably[3]. Hydrogen incorporated amorphous semiconductors are called hydrogenated amorphous semiconductors. Owing to its importance both in technology and science, the study of hydrogenated amorphous silicon (a-Si:H) has become a field by itself.

1.3 Aspects of Amorphous Silicon Schottky Barriers :

Hydrogenated amorphous silicon, a-Si:H, is a unique semiconductor in its own right. The properties of metal contact on a-Si:H present a series of questions at the basic science level and many technological challenges. The aspects that are clearly identifiable are the role of band tail states and the defects in the gap. In fact, the most useful material is the undoped a-Si:H which exhibits a near midgap Fermi energy. Doping of a-Si:H either

p- or n- type causes large increase in DOS (in the gap), which leads to carrier recombinations. Therefore, the carrier lifetime is significantly larger in case of undoped material as compared to doped a-Si:H. Thus the Schottky barrier of most interest is formed on undoped material. Of course, stable and reproducible a-Si:H can be produced in which the Fermi level (E_F) can be shifted through substitutional doping. The properties of metal contacts on doped a-Si:H also are of significant importance.

1.4 Schottky Barrier Formation on a-Si:H :

Schottky diodes on a-Si:H were first produced[4] in 1974 with first report of well characterized barriers by Wronski *et al*[5] in 1976. A schematic of the band structure for Schottky barrier is shown in Fig. 1.2. The schematic assumes a density of surface states (DOSS) for a-Si:H. Thus even when the metal and semiconductor are electrically separated as in Fig. 1.2a, there will be a band bending at the surface. An unusual aspect of this configuration is that the electrical neutrality is maintained by ionized centres near midgap. This is to be contrasted[6] with crystalline silicon (c-Si), in which the ionized donors or acceptors lie near the band edges.

The Schottky barriers are formed when the metal and semiconductor are brought into equilibrium and intimate contact[7]. This is shown in Fig. 1.2b and 1.2c. In Fig. 1.2a, the metal and

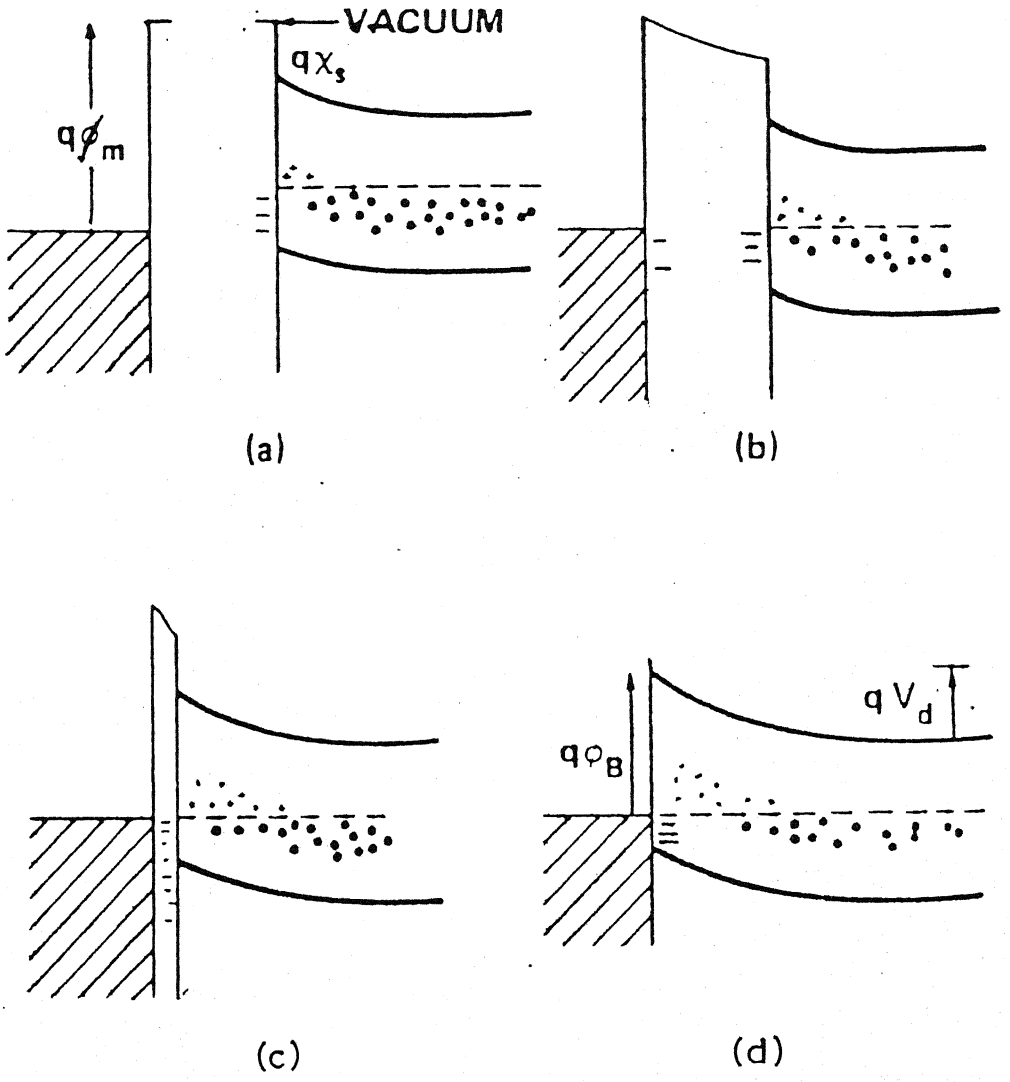

Fig. 1.2. Schematic of Schottky barrier formation for a metal and a-Si:H: (a) isolated metal from the a-Si:H; (b) and (c) they are in electrical equilibrium; (d) in intimate contact.

semiconductor are well separated but they are in electrical contact assuming that a wire connects the two. Electrons will then be transported to metal surface, which will establish a potential such that the Fermi energy of the two materials are equivalent. The slanted line between the metal and semiconductor represents potential due to the charges. These charges are balanced by additional ionized centres that will occur near the semiconductor surface. As the distance between the metal and semiconductor is decreased, more charge is transported to the metal surface. When the magnitude of the transported charge becomes comparable to the surface defects density on the semiconductor, then band bending will occur. The configuration shown in Fig. 1.2c may equally represent the case in which an oxide or insulator exists between metal and semiconductor.

The schematic shown in Fig. 1.2d then represents the Schottky barrier after intimate contact. In semiconductor, the bands are bent due to the ionized centres near the surface. This give rise to built-in potential (V_d) of interface. In crystalline silicon (c-Si), the extent of band bending region is called depletion region, referring to the concentration of majority carrier near the surface. Of course, as the metal and semiconductor are brought into contact, chemical reactions[8-11] can occur, causing changes in the properties of the Schottky barriers.

1.5 Barrier Profile in a-Si:H Schottky :

We now turn to the considerations about the depletion regions. While solution of general gap states distributions are difficult to obtain, two cases which typify different possibilities can be solved exactly. The solutions yield a parabolic band for single donor or acceptor band (as is usually the case in c-Si) and exponential behaviour for the continuous uniform-state density. These two cases are illustrated in Fig. 1.3. The field dependence of the two cases also differ. For the discrete level, a linear dependence results whereas an exponential behaviour is obtained in the uniform density of state case. For amorphous semiconductors, a uniform distribution of states in the gap is often considered as a reasonable approximation[12], and this results in an exponential potential distribution $V = V_d \exp(-x/x_0)$, where x is the distance from interface, x_0 defined as field decay length. The depletion region is no longer well defined, but often V_d/e point is used to demark the depletion region.

It should be noted that a-Si:H exhibits a DOS that is neither constant nor discrete[6]. Deep level transient spectroscopy (DLTS)[13], optical absorptions[14], and photoconductivity[15] measurements have indicated that a rather broad defect band lies in the gap and is centred below the Fermi energy. This means that for the case in which the built-in potential (V_d) is less than the

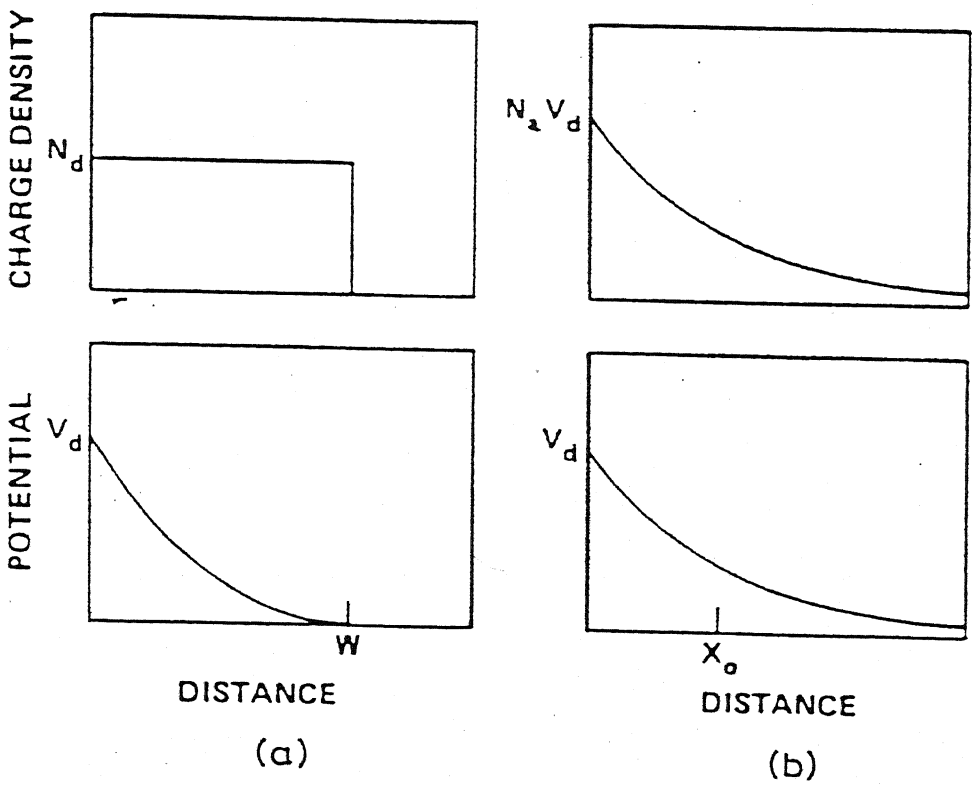

Fig. 1.3. A schematic of the charge density and potential profiles of the depletion region for a semiconductor with (a) a single donor band and (b) a uniform distribution of donors through out the gap.

width of defect band (W_d), the exponential behaviour[12] will be expected. On the other hand if diffusion potential is greater than defect band width (for metals with larger work function, ϕ_m) bands will exhibit a combination of exponential and parabolic behaviour. Near the metal-semiconductor interface the potential will be parabolic while at the far end of the space charge region the potential will be exponential.

The Schottky barrier height for ideal crystalline case is often written as difference between the metal work function (ϕ_m) and semiconductor work function (ϕ_s), that is $\phi_b = \phi_m - \phi_s$.

Whenever there is a large density of surface states, the semiconductor Fermi level gets pinned[16] at the neutral charge level (ϕ_0) at the surface, making ϕ_b independent of the metal work function. In this situation ϕ_b is given as $\phi_b = E_g - \phi_0$, E_g the gap energy. But in case of amorphous Schottky barrier, because of the presence of large DOS in gap it is difficult to predict the form of Schottky barrier height expression.

There are several factors which modify the Schottky height. The most inherent is the image force lowering[16], which occurs when an electron transits the depletion region. This does not depend upon the presence of the interfacial oxide layer and occur even when such a layer is not present. When the electron is at some distance in the depletion region there exists an electric field which can be calculated considering an image charge located at the

same distance in metal. This field causes the effective barrier to be reduced, and maximum will occur at several nanometre into the semiconductor instead of the surface. The magnitude of lowering is proportional to the one fourth power of band bending. Thus measurements like current-voltage (I-V) or internal photoemission (IPE) where electron transition over barrier across the depletion occurs, will reflect the image force lowering of the barrier. In contrast, measurements like capacitance-voltage (C-V) are not made in presence of transiting charge and will not be affected further. Since the barrier maximum occurs away from the interface, weak effects due to bias variations are possible.

Another factor, mentioned earlier, that the density of surface states affects the ϕ_b formation and makes it almost independent of ϕ_m, by pinnimg E_F at the surface. But the origin and the nature of these states still remain enigmatic. An advanced study argues that the pinning of states are associated with the semiconductor alone and are related to metal-induced gap states[17,18], defects[19,20] at or near the semiconductor surface. More recent studies have thrown a new light on the formation

mechanism of Schottky barrier, and shown that in metal-semiconductor contact, E_F pinning is possible to either the valence band or the conduction band of semiconductor[21]. The metal as well as semiconductor wave functions also influence the

interface states[22-25]. Thus density and energetic position of interface states strongly depend on the metal[22-25].

Therefore it is clear form the above discussion that the formation of Schottky barrier and its height, both are affected predominantly by DOS in gap, interface states, electric field at the junction and metals.

1.6 Carrier Transport Through a-Si:H/metal Interfaces:

It is now appropriate to briefly review the basic mechanisms through which carrier transport across the Schottky barrier results. These mechanisms can be categorized on the basis of the barrier height faced by the various processes. These in comparison with crystalline semiconductors are illustrated in Fig. 1.4. The schematic represents a Schottky barrier on an undoped a-Si:H under forward bias. At room temperature, it is usual to consider that the electron transport over the barrier dominates the forward-bias current. For high mobility materials such as c-Si, it is presumed that the electron population at any energy above conduction band minimum (E_c) is independent of distance (x) from the surface. The transport is limited by the emission of electron into metal. For low mobility materials it is possible that current transport is limited by electron diffusion theory (DT) through the depletion region. In this case, the population at any energy will vary as a function of distance from the surface. Thus if thermionic emission

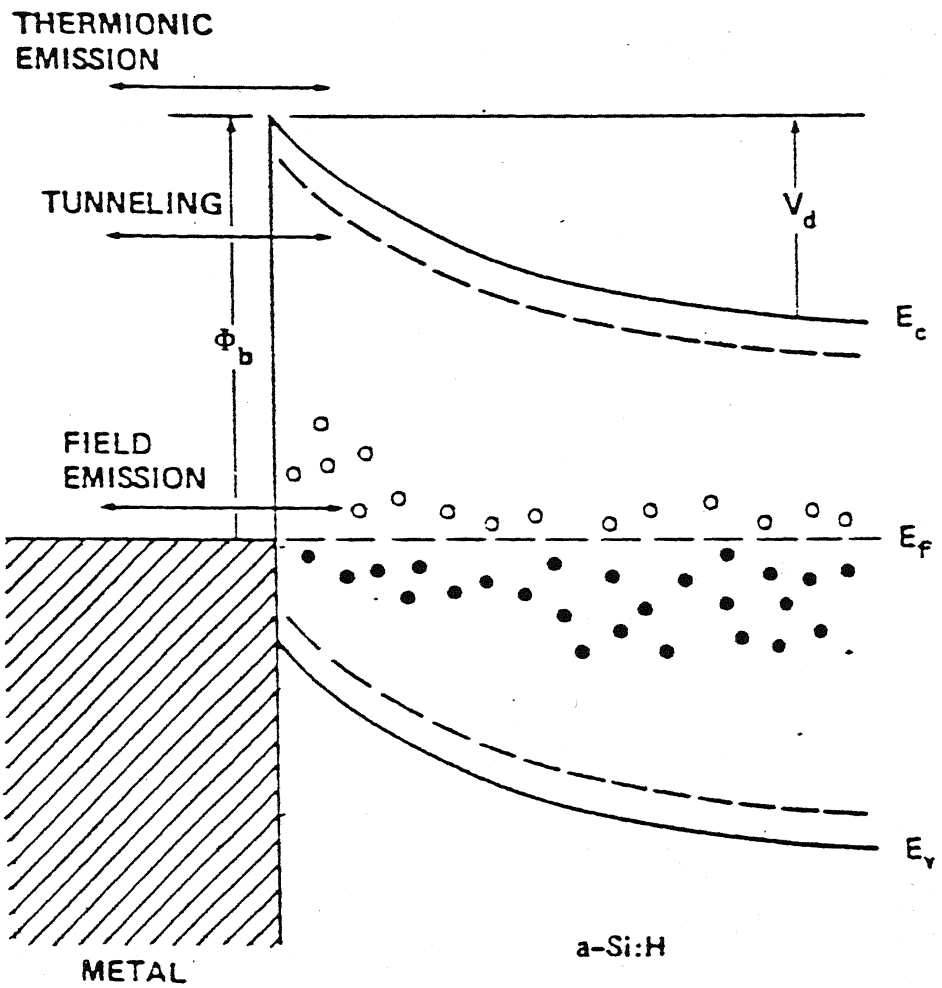

Fig. 1.4. Schematic of the Schottky barrier on a-Si:H showing the different transport mechanisms.

theory (TET) limits the transports then for an applied forward bias the E_F will be constant throughout the depletion region and drop to the metal film. In contrast, for diffusion limit transport, E_F will vary in the depletion region. Because a-Si:H has low mobility ($\approx$ 2-4 $cm^2V^{-1}sec^{-1}$) it is not clear which mechanism will dominate. In fact, both mechanisms have been reported by different authors[26-30]. In fact, there remains a debate on the actual carrier transport mechanism across the Schottky barriers.

At a low temperature (T), tunneling currents may become more important. The tunneling of electrons from conduction into metal is certainly observed in crystalline silicon, and has also been reported for a-Si:H[27,31]. This process is more complicated in a-Si:H because the localized states near conduction band tails may significantly enhance the tunneling currents.

Field emission is a much less likely path in a-Si:H Schottky barrier under forward bias. Since E_F is near midgap, there is a relatively low DOS and states are localized. Thus there are few states that can give rise to field emission into the metal. In reverse bias field emission breakdown[28] can be observed due to the emission from the metal Fermi energy into the a-Si:H conduction band. For lightly doped a-Si:H, field emission is observed at higher reverse bias, where as highly doped a-Si:H exhibits field emission at relatively lower reverse bias.

Since the Fermi energy is near the midgap, as mentioned earlier, minority carriers (holes for undoped a-Si:H) can play significant role. This is especially true for low metal work functions. Although the minority carrier concentration may be higher than c-Si diodes, it can still be neglected for most analyses.

1.7 Plan of The Present Work:

Knowledge of electronic properties of the metal/semiconductor contacts is of crucial importance for the basic understanding of the Schottky barrier formation. Over the last 15 years, numerous studies regarding the metal/a-Si:H Schottky barriers have been developed. It is evident from the previous discussions so far, that there are still contradictory reports on the carrier transport mechanisms in Schottky diodes. Efforts have been made to characterize the transport mechanism and both thermionic emission and diffusion have been proposed. Thus there remains a controversy on whether the dark I-V characteristics, under forward bias, is governed by the diffusion limited transport or thermionic emission limited transport. As the determination of barrier height strongly depends on what carrier transport theory being used, it is necessary for the proper characterization of the metal/a-Si:H contacts to identify the most dominant mechanism working in a-Si:H Schottky diodes. The usual practice of calculating the barrier

height of a-Si:H Schottky diodes uses the saturation current, I_s's, obtained from the extrapolation of dark I-V curves is not a reliable method of characterizing the Schottky junction. This is because the usual exponential equation $I=I_s[\exp(qV/kT)-1]$,deviates from the experimental dark I-V data. This discrepancy between theory and experiment is attributed to the high dark bulk resistance of undoped a-Si:H. To minimize this effect in ϕ_b determination, I_s is derived from the linear fit of $\ln(I_s)$ vs V (1) to a limited number of I-V data points at lower biases, where bulk series resistance effect is considered negligible. However the choice of range of data points for this linear fit involves a lot of subjectivity. To avoid such complexity, Wronski *et al*[32] havesuggested an alternative way of finding I_s from the dependence of short circuit current, I_{sc}, and open circuit voltage, V_{oc}, on the intensity of volume absorbed light. It, however, becomes problematic at higher temperatures where V_{oc} goes down to as low as the thermal energy of the carriers (3kT/q).

We, therefore, have undertaken a comprehensive study of dark I-V characteristics under forward bias, and tried to make it more trustworthy for its traditional use for the determination of barrier height of Schottky diodes on a-Si:H. Chapter III is fully devoted to this goal.

Further, ac behaviour of Schottky diodes on a-Si:H is the most important to understand its device properties and material

properties as well. Various complex models have been advanced to explain and predict ac behaviour. Improvements are still going on to get a simple predictable model. We have given details of capacitive behaviour in chapter IV.

Finally the system gold/a-Si:H has received a special interest[33]. Because of its important applications in practical devices, and because it is a fundamental and attractive subject, a growing interest in formation of Au Schottky barriers on a-Si:H has developed recently.

CHAPTER II
EXPERIMENTAL TECHNIQUES

This chapter gives the details of experiments, and describes the principle and measurement procedures. Thin metallic films of Au are deposited, by thermal evaporation under high ($\leq 10^{-5}$torr) vacuum, on freshly etched and clean undoped a-Si:H surface. Dark and photo I-V measurements are taken at various temperatures under high vacuum. Internal photoemission of electrons into the a-Si:H is carried out under different biases. Static capacitance and conductance measurements as a function of both frequency and bias are performed at room temperature.

2.1 Sample Description:

We took well characterized undoped a-Si:H thin film[34]. It was of low DOS ($\sim 4X10^{15}cm^{-3}eV^{-1}$)[35] near midgap and prepared by dc glow discharge decomposition of pure silane. About ≈ 200 Å thick layer of n^+a-Si:H was deposited on top of the glass substrate, precoated with indium tin oxide (ITO) as back contact, to act as a good ohmic contact to the subsequently deposited undoped a-Si:H layer having thickness of ~ 4 μm. We thus got the sample in Glass/ITO/n^+-i-a-Si:H structure.

2.2 Fabrication of Schottky Barriers:

The fabrication of good Schottky barrier requires the semiconductor surfaces to have intimate contact with metal. For this purpose, the surface of a-Si:H was first etched by dipping it into 10 Vol.% electronic grade hydrofluoric acid (HF) in methanol for about half a minute to remove the native oxide layer grown due to the surface reactivity of the film even at ambient temperatures. Then it was quickly rinsed in deionized water to prevent further etching. This process was repeated few times till the native oxide was completely removed. Then the film was rinsed in electronic grade methanol. The etched and rinsed a-Si:H film was transferred into the vacuum chamber of the coating unit. Fig. 2.1 shows the coating unit used which contains an oil diffusion pump and a liquid nitrogen trap. Then the a-Si:H film was dried at $50^{o}C$ and annealed at $230^{o}C$ under the base pressure $\leq 10^{-5}$ torr for half an hour. After this it was cooled down slowly to room temperature under high vacuum. About 50 mg pure gold was cleaned, dried and deposited on masked a-Si:H film by thermal evaporation. A shutter was used to avoid pre-deposition of impurities at the top of a-Si:H surface. Thus the Schottky barrier of typically 1.5mm to 2.0 mm diameter gold (Au) dots were prepared by vacuum thermal evaporation of semitransparent ($\sim$ 70 - 100 Å thick) Au metal. At the time of deposition the substrate temperature was maintained at $\sim 50^{o}C$. The Schottky barrier, sandwiched structure

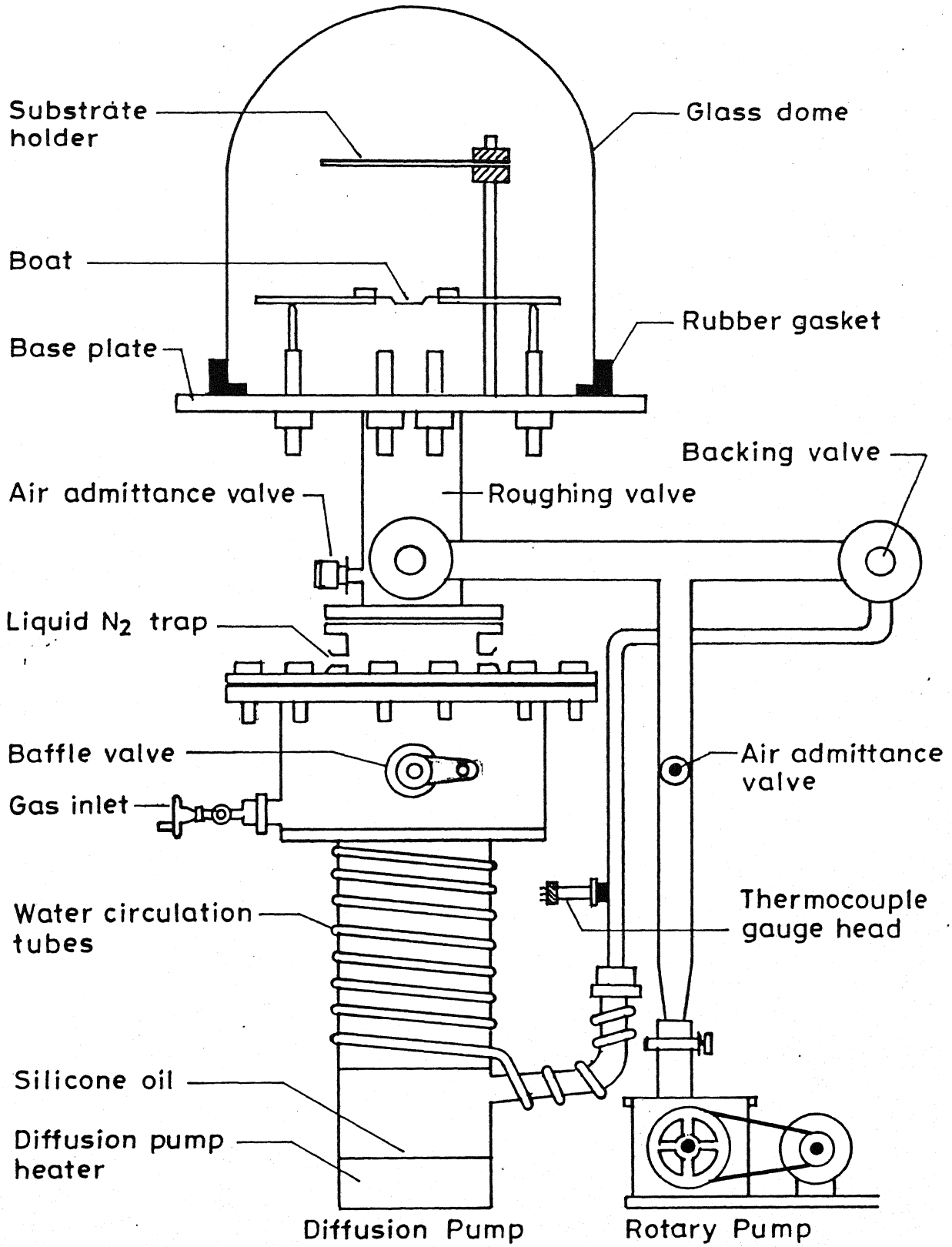

Fig. 2.1. Schematic of the thermal evaporation set up.

thus obtained, is shown schematically in Fig. 2.2.

2.3 Current - Voltage (I-V) Measurements:

We have measured dark and photo I-V characteristics at room temperature (298 K) and dark I-V as a function of temperature, in the range from 269 K to 417 K using a liquid nitrogen cryostast which is shown in figure 2.3. The sample temperature was measured by a copper- constantan thermocouple attached near the sample on the brass block which contains a heater to heat the sample and a passage for liquid nitrogen (or water flow). For good electrical ohmic contacts two specially designed probes, one of gold and another of copper wire with spherical point tips, were used. The whole thing was then covered by a black metallic belljar, having a glass window on the top through which light can be shone on the sample. All the measurements were taken under vacuum better than ~ 10^{-5} torr.

For photo measurements light was shone from a 100 watt tungsten halogen lamp having intensity of ≈ 34mW cm^{-2} on the sample top glass window. The open circuit voltage (V_{oc}) and short circuit current (I_{sc}) were measured by Keithley model 617 electrometer. Neutral density filter were used to vary the intensity of incident light on the sample. In case of I-V measurements at a fixed temperature, diode current was measured at different dc biases ranging from -2.0 V to +2.0 V using the same

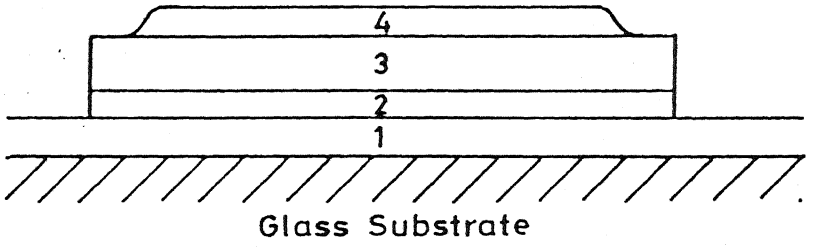

Fig. 2.2. Schematic section through sample: (1) indium tin oxide bottom contact; (2) n^+ a-Si (≈ 200 Å); (3) a-Si:H (≈ 4 μm) ; (4) gold top contact (≈ 50 - 100 Å). Sample area ≈ 3 mm^2.

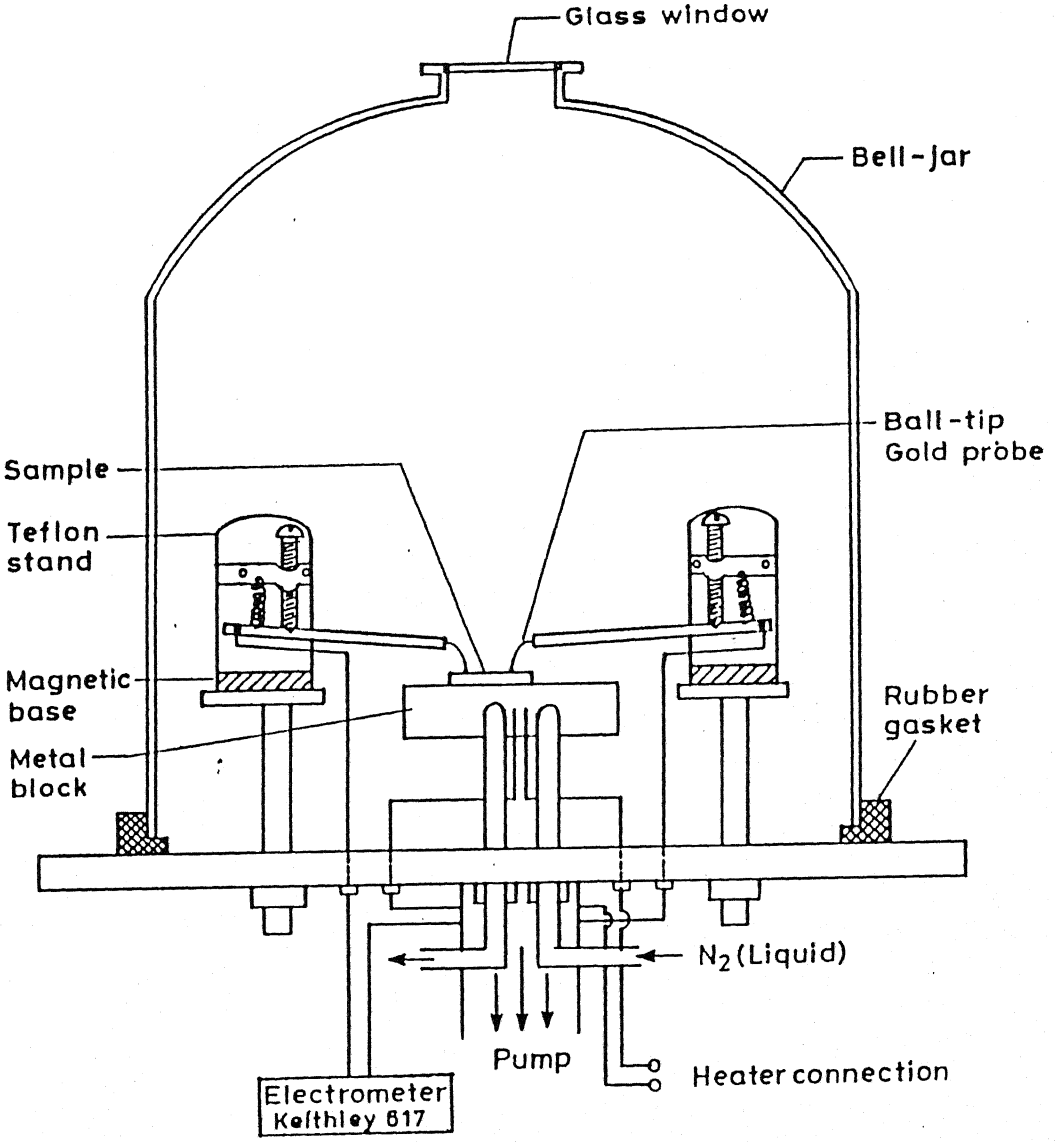

Fig. 2.3. Schematic of the liquid nitrogen cryostat. (not in proper scale)

Keithley model 617 electrometer and its inbuilt voltage source. For below room temperature measurements liquid nitrogen was passed through the sample holder at a controlled rate, whereas for high temperatures the sample was heated using a heater under controlled rate. The thermocouple voltages were measured using Keithley model 197 multimeter. The temperature was allowed to rise slowly. The system was allowed to have its electronic processes fully in thermal equilibrium keeping it at a desirable fixed temperature for about 15 - 20 minutes before any measurement at that temperature was done.

2.4 Internal Photo Emission (IPE) Measurements:

Internal photo emission is considered as the most reliable method for Schottky barrier height (ϕ_b) determination. A well calibrated ORIEL tungsten -arc-halogen lamp fitted with grating, which provides reasonable intensity light over wide range of wavelength from 600 - 1400 nm was taken as light source. A calibrated Si-photodiode sensitive to the wavelengths (λ) ranging from 700 - 1100 nm, was used for intensity measurements. A thin a-Si:H film was used as filter to exclude all the wavelengths 700 $< \lambda >$ 1100 nm thus minimizing the stray light effects. The photo currents at a particular bias were measured with different incident photon energies $1.13 \leq E \leq 1.77$ eV, using Keithley model 617 electrometer and its inbuilt voltage source. When the bias

voltage was changed, about half an hour was given to any slow process for relaxing before further measurement was made. The same reading was taken for different dc bias ranging from +1.0 V to -2.0 V.

2.5 Capacitance and Conductance Measurements:

The details of this technique are discussed in Chapter IV.

CHAPTER III

CARRIER TRANSPORT IN SCHOTTKY BARRIERS

This chapter describes the results and discussion on determination Schottky barrier height, ϕ_b. Here we first explain the theory of each individual measurement technique and proceed to experimental results and their discussions. The ϕ_b, obtained directly from the dark I-V characteristics measured as a function of temperature, is quite low (0.82 eV for diffusion theory), which is discussed in the section 3.1. This low value of ϕ_b is found to be due to some unknown leakage currents which are extracted out by a simple model for computer simulation along with the bulk resistance, R_s, of the a-Si:H. This model offers us excellent results for I_s, comparable to the value obtained from I_{sc}-V_{oc} measurements as a function of intensity of volume absorbed light, and thereby yields accurate ϕ_b (0.89 ev for diffusion theory). It also gives the approximate bulk activation energy, E_a, using series resistance obtained from simulation, a complete picture of which is given in section 3.2. Finally section 3.3 is devoted to internal photoemission measurements which can be considered as crucial in identification of the actual carrier transport mechanism over a-Si:H Schottky barriers. IPE gives most reliable and accurate ϕ_b. Therefore, transport mechanism which gives ϕ_b close to that obtained from IPE measurements should be

the most dominant at the Schottky barrier junctions. We argue here that the diffusion theory is the likely carrier transport mechanism over the Schottky barriers on a-Si:H.

The characteristic parameters used to characterize a Schottky barrier are the barrier height (ϕ_b), ideality factor (n),reverse saturation current (I_s) as a function of reverse bias (V_r), and bending potential (or diffusion potential,V_d). Some of these are called static parameters which deal with the potential distribution, and some are transport parameters which relate to the movement of carriers between the semiconductor and metal, and others are known as mixed parameters which include both static and transport behaviour.

In this chapter we are concerned with extraction of these Schottky diode parameters and interpretation of results so obtained.

3.1 Current-Voltage (I-V) Characteristics:

3.1.1 Theory of I-V Characteristics:

The forward-bias I-V characteristics is the most used method of characterizing a semiconductor junction. Moreover, because of the high resistivity (ρ) of undoped a-Si:H, I-V measurements proved to be the most reliable method of determination of Schottky barrier height (ϕ_b). In the case for crystalline semiconductor[16], the Schottky diode equation can be written as

$$I = I_s \exp(qV/nkT)\,[1 - \exp(-qV/kT)] \quad \ldots\ldots\ldots (1)$$

where I_s is the reverse saturation current, n the ideality factor, q the electronic charge and k the Boltzmann constant. This equation is usually written as

$$I = I_s \exp(qV/nkT) \quad \ldots\ldots\ldots\ldots\ldots (2)$$

and this expression is a good approximation for $V > 3kT/q$. These equations upto this point are independent of whether the current transport is thermionic emission or diffusion limited. The behaviour of ideality factor n can lead to some insight regarding the current transport mechanism[16,7]. For instance, if the forward-bias current transport across uniform metal/semiconductor junction is limited by thermionic emission theory, then n will be near unity. If, however, the transport is diffusion limited, the recombination in depletion region can then cause n to vary between 1 and 2. The details of diffusion limited transport have been modeled by Chen and Lee[36]. It should, however, be noted that even if the current is diffusion limited but no recombination occurs in depletion region n will still approach unity. For junction due to inhomogeneities, the barrier height may vary from place to place and the I-V measurements will exhibit a high n value [37]. Although all of the transport processes may be occurring in Schottky diodes, the I-V measurements will usually be dominated by one of the mechanisms which provides the highest resistance to the transport. Besides recombination and diffusion-limited transport,

there are several other effects like -interface layer, lateral inhomogeneities and field dependence of the barrier which increase the value of n.

If the forward-bias characteristics are predominantly due to thermionic emission then,

$$I_s = A\, A^{**}\, T^2 \exp(-q\phi_b/kT) \qquad \ldots\ldots\ldots\ldots\ldots\ldots (3)$$

where A is the effective area of the diode, ϕ_b the effective Schottky barrier height (including image force lowering), and A^{**} the Richardson constant corrected for electron diffraction and reflection at the barrier. Thus to obtain ϕ_b it is necessary to measure the temperature dependence of I_s and then plot $\ln(I_s/T^2)$ vs 1/T which should result in a straight line. This slope will yield ϕ_b.

If the crrier transport is diffusion limited then the temperature dependence of I_s is given by

$$I_s = q\, N_c \mu\, E_\mu \exp(-q\phi_b/kT) \qquad \ldots\ldots\ldots\ldots\ldots (4)$$

where μ is the electron mobility, E_μ is the maximum field at the surface, and N_c is the effective density of states (DOS) in the conduction band (CB). Hence a plot of $\ln(I_s)$ vs 1/T can be used to verify diffusion-limited transport mechanism and the slope will yield ϕ_b.

3.1.2 I-V Results:

Fig. 3.1 shows the log(I) vs V plots at room temperature (298 K) for both forward and reverse bias. This clearly indicates very good Schottky behaviour with high rectification ratio (~ $4X10^{5}$ at 2.0 V dc bias voltage), I_s = $2.1X10^{-12}$Amp, and the ideality factor (n) equal to 1.28. Since the good quality undoped a-Si:H has very high resistivity, n obtained from I-V measurements is not much accurate. To overcome this we used short circuit curren(I_{sc}) and open circuit voltage (V_{oc}) relation[38]:

$$I_{sc} = I_s \exp(qV_{oc}/nkT)$$

which is, at room temperature, illustrated in Fig. 3.2. In this case n = 1.10 and I_s = $1.50X10^{-12}$Amp. This low value of n indicates the high quality of Schottky barrier junctions fabricated by us.

Figs. 3.3 and 3.4 show current-voltage characteristics as a function of temperature under forward and reverse bias conditions, respectively. Reverse bias currents at temperatures below < 298 K are too low to measure accurately. So reverse bias I-V characteristics are not shown. These plots also show a good Schottky diode behaviour with slow decrease in n-values throughout the temperature range. Ideality factor,n, obtained from dark I-V plots, lies between 1.1 to 1.4 in the temperature range from 269 K to 417 K. Now Fig. 3.5 illustrates both log(I_s) vs 1/T and log (I_s/T^2) vs 1/T plots with I_s values obtained from the

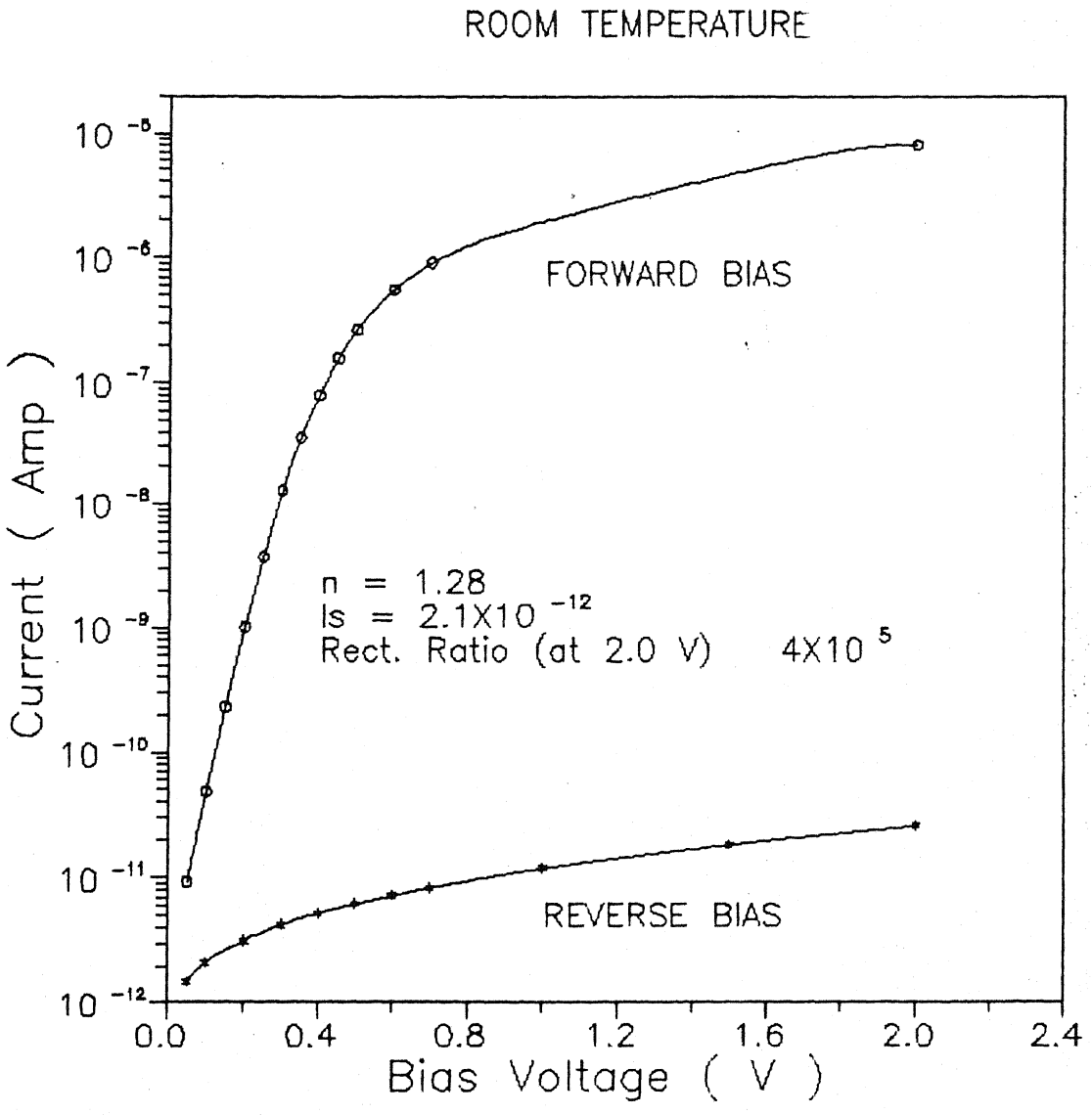

Fig. 3.1. The forward bias and reverse bias I-V characteristics measured at room temperature.

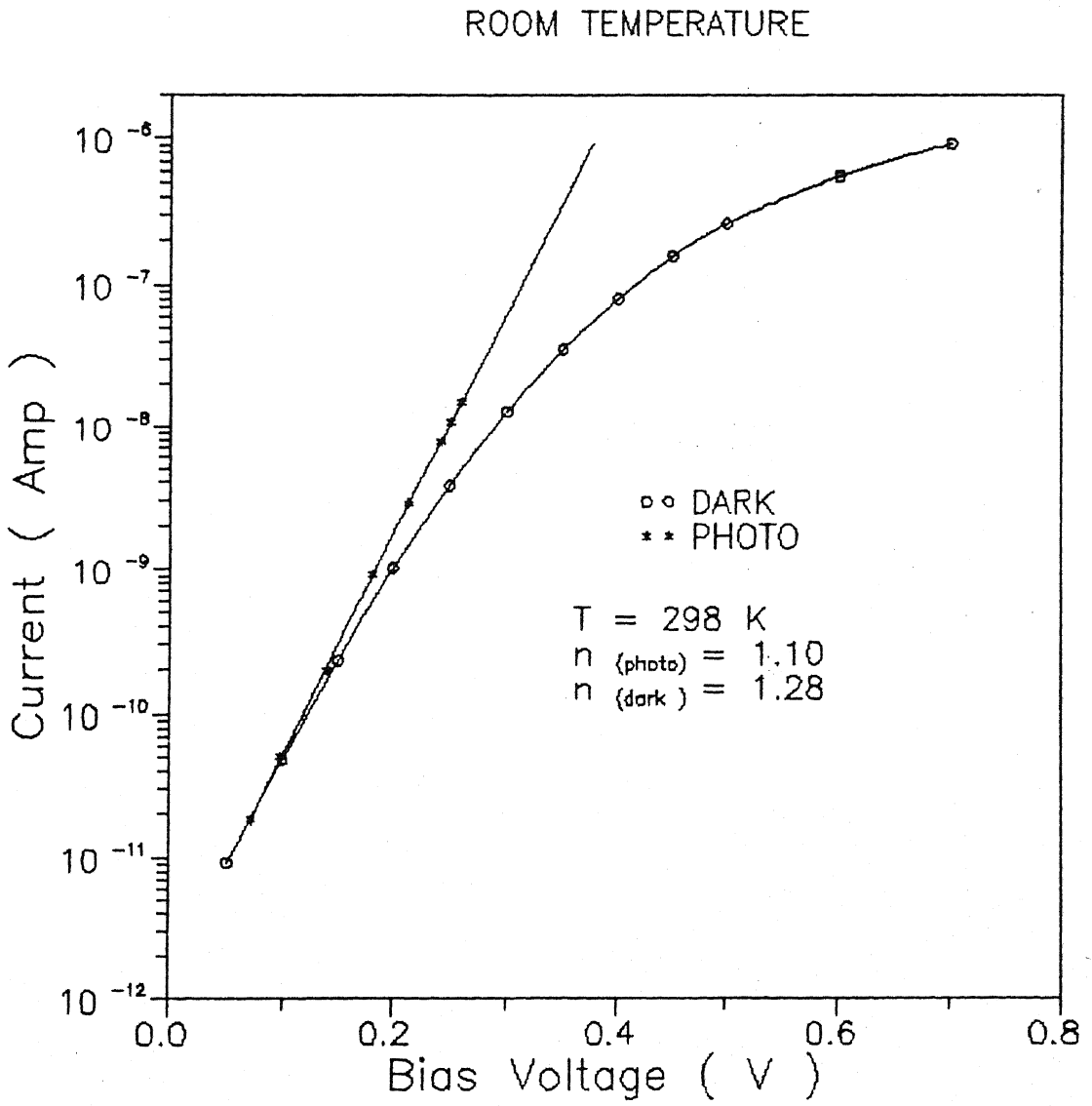

Fig. 3.2. The characteristics of forward bias dark I-V and light I_{sc}-V_{oc} measured as a function of light intensity.

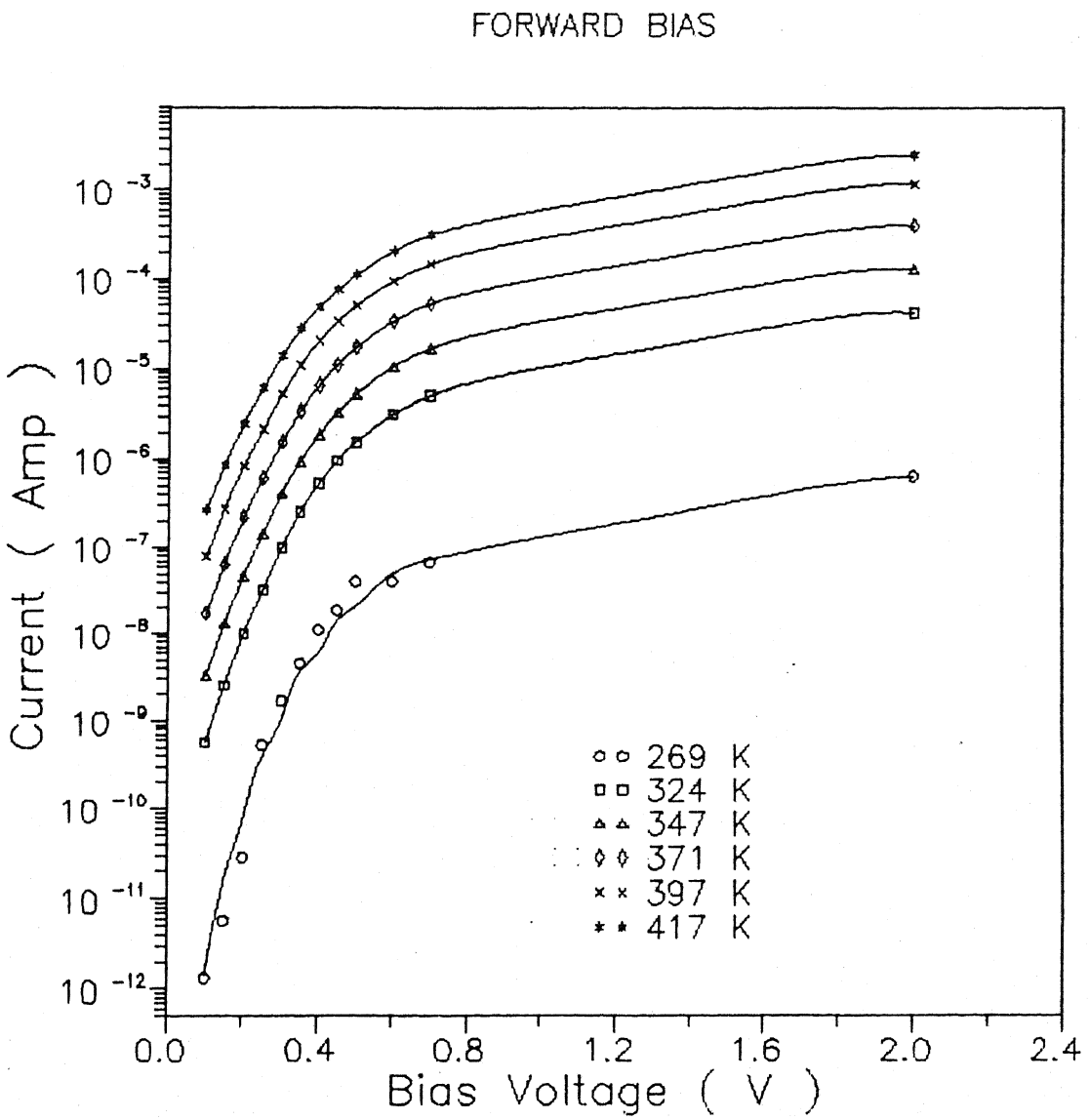

Fig. 3.3. The forward-bias characteristics of dark I-V measured as a function of temperature.

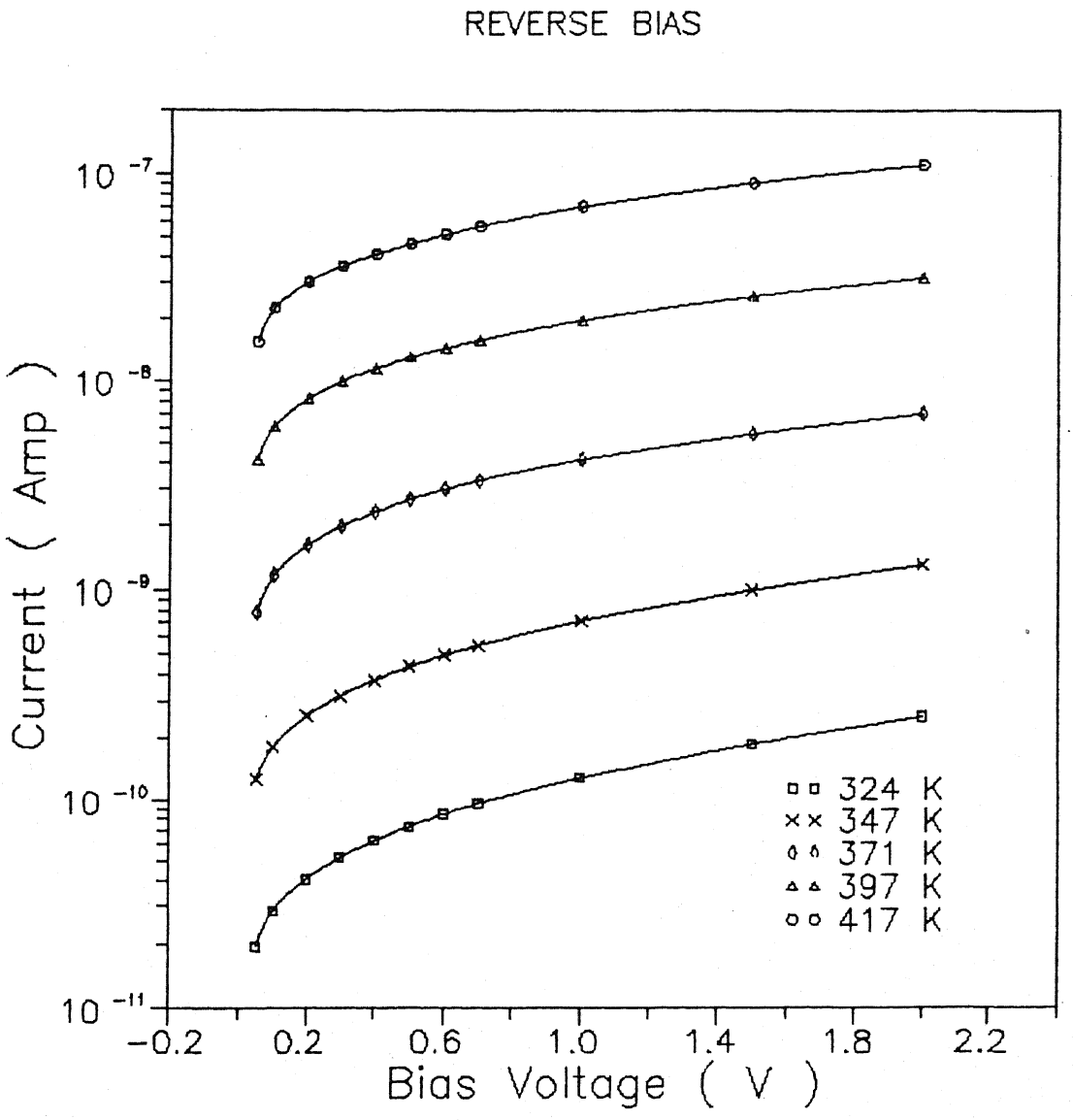

Fig. 3.4. The reverse bias characteristics of dark I-V measured as a function of temperature.

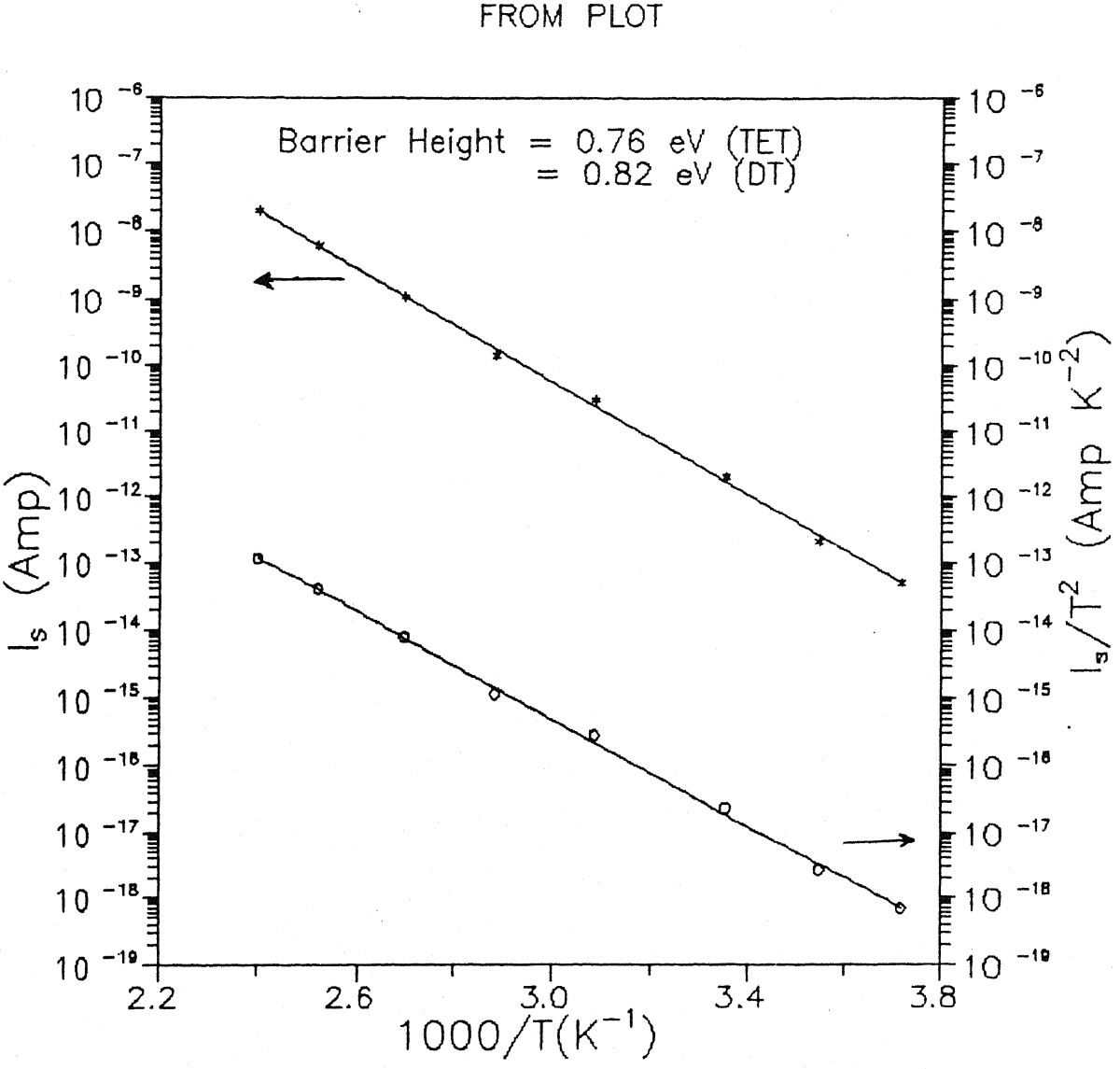

Fig. 3.5. The extrapolated value of dark forward current (I) plotted in both thermionic emission theory (circles) and diffusion theory (stars).

extrapolation of forward log(I) vs V curves to current axis at V = 0. The values of barrier height obtained using two different mechanisms differ by about 0.06 eV; ϕ_b = 0.76 eV for thermionic emission theory and ϕ_b= 0.82 eV for diffusion theory. Here we should notice two important points: first, the value of Schottky barrier height, ϕ_b is less than expected, and secondly the extrapolated I_s fits equally well to both the thermionic emission and the diffusion limited theory. Thus we are uncertain about the actual transport mechanism. Similar observations have been made by others[37]. However, they simply ignored it as experimental error involved in their measurements over the temperature range.

Considering the fact that due to high bulk resistance of the undoped a-Si:H, high-forward-bias-diode-current is fully controlled by it, we deduced the series resistance, R_s from high forward bias data and then fitted the exponential expression, $R_s(T) = R_0 exp(E_a/kT)$ in Fig. 3.6. This fits well and yields the activation energy, E_a, as 0.53 eV, which is quite smaller than that expected for the case of coplanar structure. In fact, this discrepancy implies that quasi Fermi level in space charge region for a Schottky diode under high forward bias deffers from the Fermi level in neutral bulk region.

Again we can see in Fig 3.2 that I-V measurements and I_{sc}-V_{oc} measurements differ in both the ideality factor, n, and saturation current, I_s. These differences had been attributed mainly to high

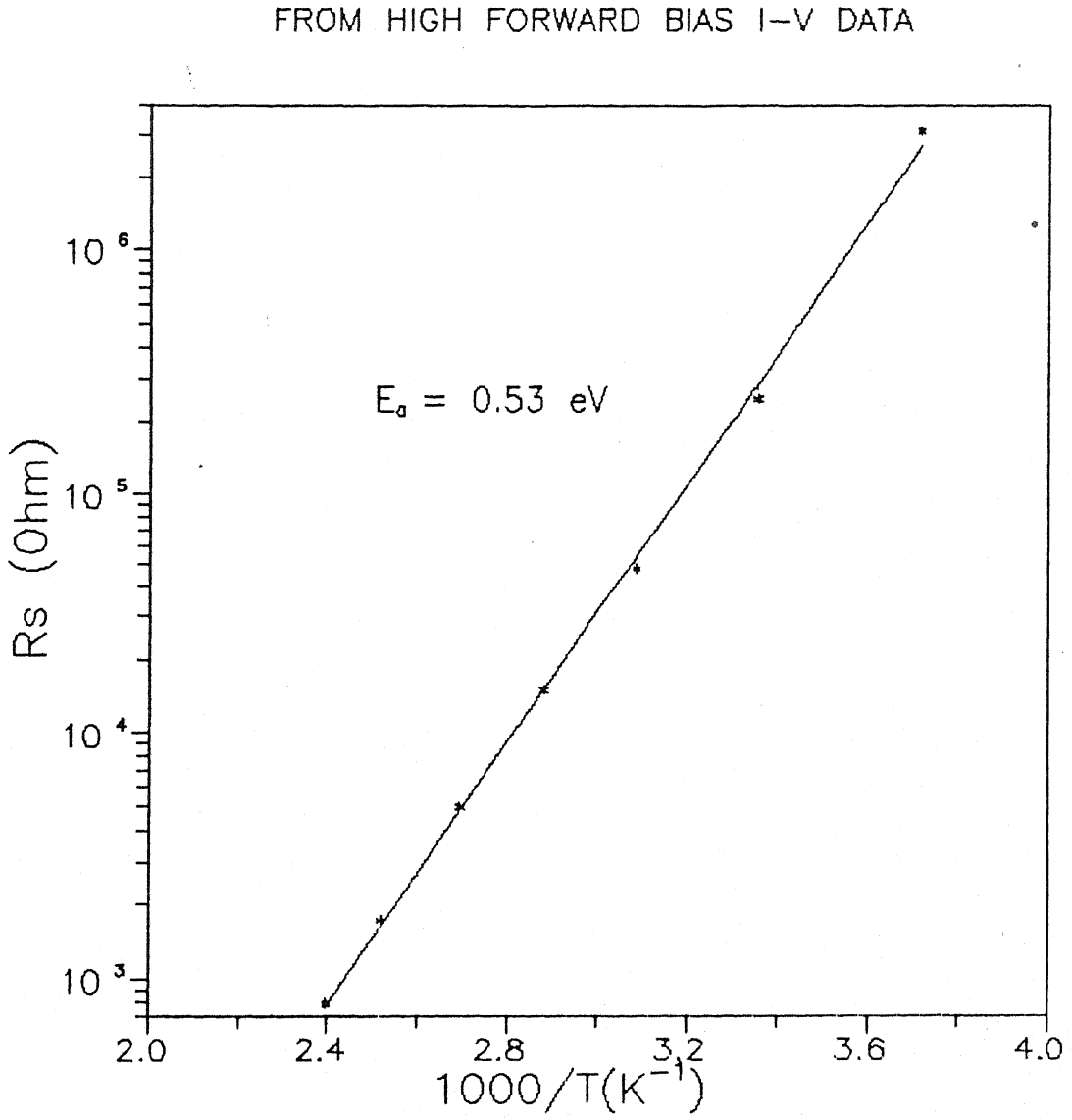

Fig. 3.6. Logarithmic plot of bulk series resistance (R_s) estimated from high forward bias I-V data vs $10^3/T(K)$.

bulk resistance, R_s. If that were the case then there should have been no discrepancy between these two measurement techniques in the bias range where the effect of R_s is expected to be quite insignificant. We, therefore, feel that during I-V measurements, some leakage currents are flowing across the barrier. For the first time we tried to separate these leakage currents so that we could get more accurate values of ϕ_b from the most used I-V measurement method.

3.2 Modeling for I-V Relationship and Simulation:

3.2.1 Development of I-V relation:

As we have seen that equation (2) does not fit experimental points for bias more than 0.2V. Thus, the barrier height found by straight line fitting of log (I) vs V becomes subjective in so far as selection of bias range used. As pointed out in the previous chapter, we used computer fitting to extract those leakage currents and parameters such as R_s which cause the deviation from equation (2). We implemented such an approach in the form of computer programme as described below. Equation used by Donoval *et al*[40] in crystalline case is

$$I = I_s \{ \exp [q (V - R_s I) / nkT] - 1 \}$$
$$+ I_g \{ \exp [q (V - R_s I) / 2kT] - 1 \}$$

But the above equation does not work in a-Si:H case because of comparatively large localized DOS in gap. These localized states increase thermally assisted tunneling. To take this into account

we have added a third term and included n for associated leakage currents, so the equation now turns into the form:

$$I = I_s \{ \exp [q (V - R_s I)/nkT] - 1 \} + I_g \{ \exp [q (V - R_s I)/2kT] - 1 \} + I_t \exp [q (V - R_s I)/E_o] \quad \text{.....(7)}$$

where I_s is same as equation (1), I_g, I_t and E_o are three leakage parameters. The former two are strongly temperature dependent and third one is very weakly temperature dependent. Second and first term of equation (7) resemble carrier recombination in depletion region and tunneling of electrons across the barrier respectively in crystalline case.

3.2.2 Simulation Procedure:

We computed the values of R_s, I_g, I_t & E_o in two steps:

1. In the first step a suitable combination of R_s, I_s ,I_g with I_t= 0, was found. For this following steps were followed.

a) After choosing a suitable range of I-V data for linear fit to equation (1) a least square fit was made in order to somewhat minimize the subjectivity involved in getting I_s from intercept at V = 0.

b) This extrapolated value of I_s and R_s obtained from high forward bias region (i.e. ohmic region) were defaulted in programme as a first approximation for the next iterations.

2. In second stage we fixed up R_s, and I_g and then a suitable

combination of I_s & I_t and obviously n was found out to fit the experimental points over wide range of forward bias (0 < V < 0.7 V) for equation (7).

Thus the saturation currents (I_s) at different temperatures were obtained. Then the value of barrier height, ϕ_b, was evaluated using both thermionic emission theory and diffusion theory.

3.2.3 Simulation Results:

Fig. 3.7 shows the computer generated curves (solid lines) fit to the experimental data (circles) at room temperature. The set of various parameters at room temperature cited in Fig. 3.6 are: n = 1.27, $I_s = 1.53X10^{-12}$ amp. These simulated results show two interesting relations: first, the value of n (=1.27) is equal to the value obtained directly from log(I) vs V plot at room temperature. second, computed I_s equals that obtained from I_{sc}-V_{oc}measurements. It ia also important to note two further points: first, since I_s obtained from I_{sc}-V_{oc} measurements results in correct value of barrier height, ϕ_b, our simulation process gives more accurate Schottky barrier height; second, the processes associated with current flowing through Schottky junctions under forward bias and under light illumination are not all the same. Fig. 3.7 shows that the computed curve exceeds the experimental curve at higher forward biases. This has been reflected throughout our wide measurement temperature range as illustrated in Fig.3.8.

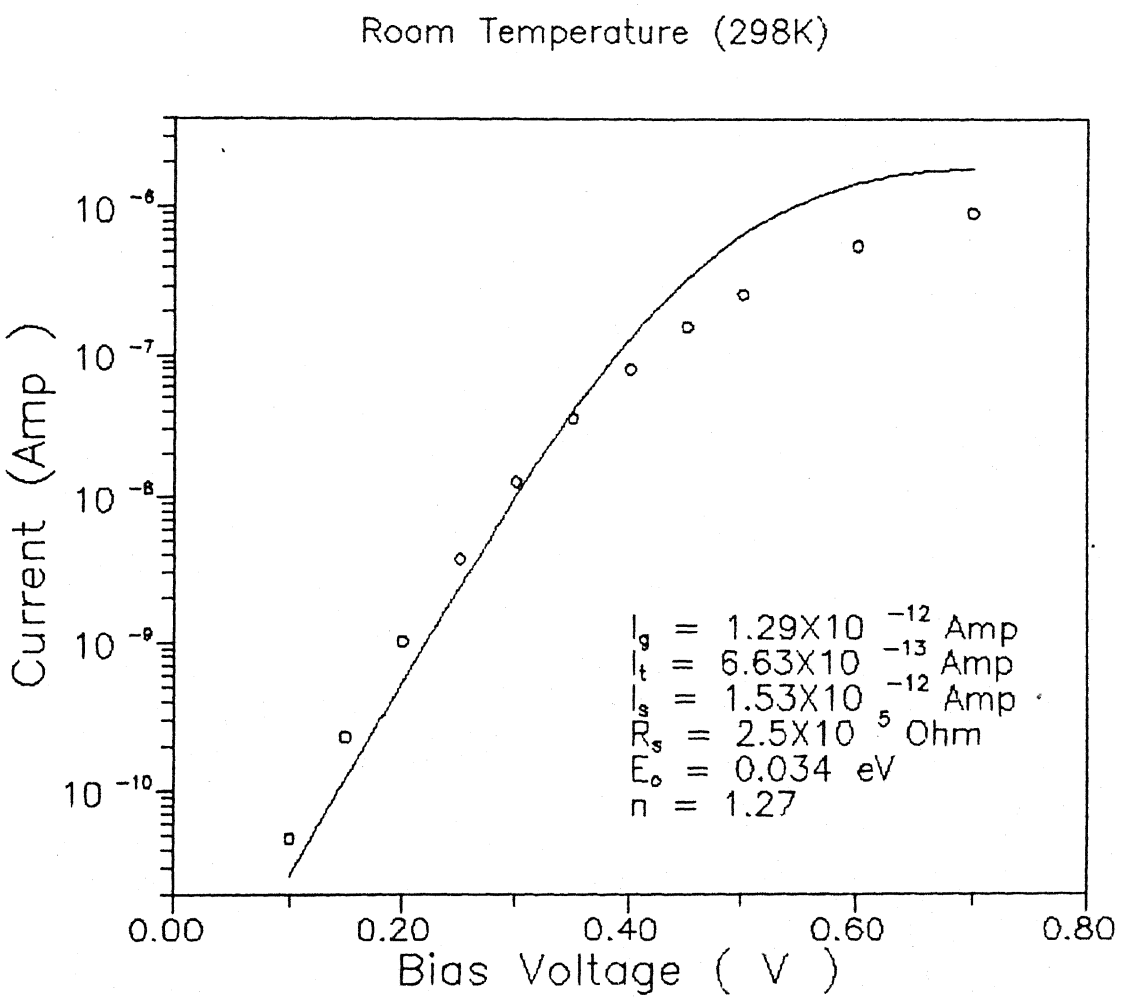

Fig. 3.7. A typical fit of the experimental room temperature I-V data (symbols) by simulation procedure (solid lines).

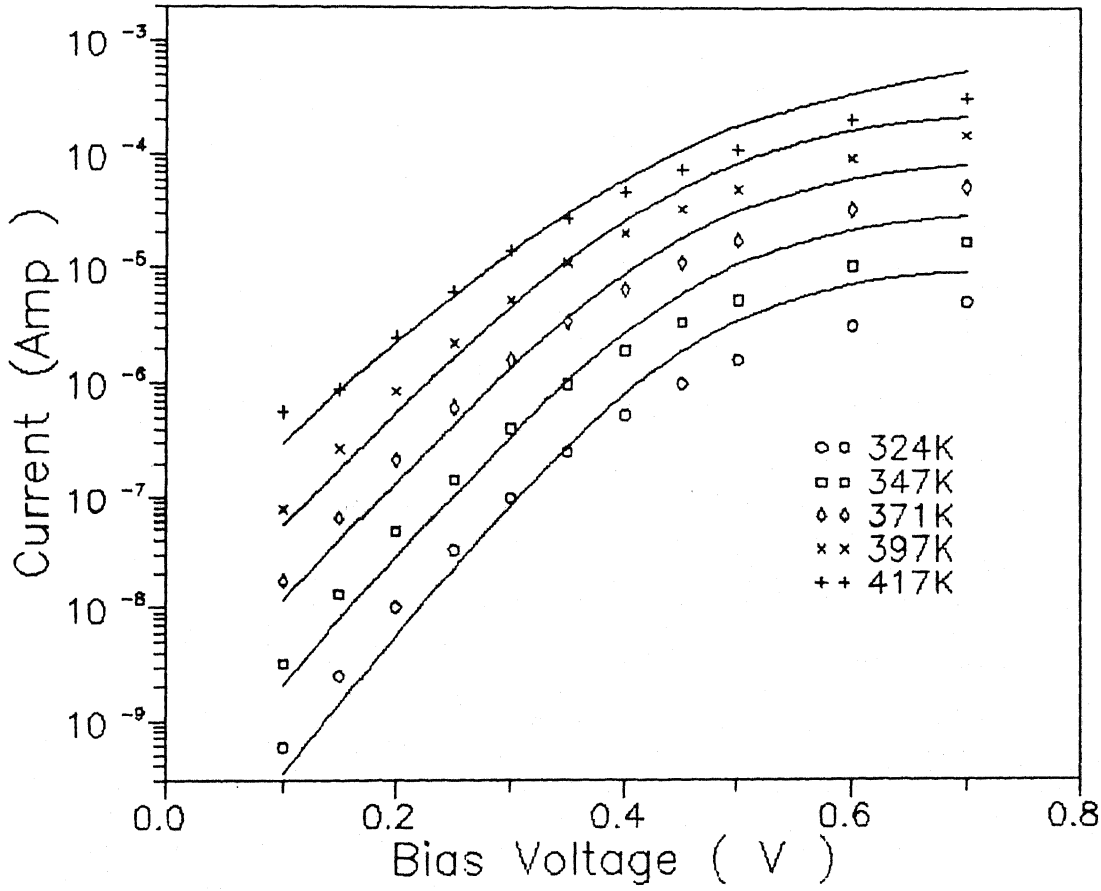

Fig. 3.8. A comparison of computer generated I-V curves (solid lines) with experimental forward bis I-V characteristics measured (symbols) as a function of temperature.

This can be due to the bias dependence of R_s, which the equation (7) did not take into account. The results obtained in the simulation are summarized in the tables 3.1 and 3.2.

The saturation current, I_s and the series resistance, R_s , as expected,are strongly temperature dependent. Fig.3.9 depicts the diffusion theory and the thermionic emission theory fit to the simulated I_s while the $\log(R_s)$ vs 1/T curve is illustrated in Fig. 3.10, which yields the activation energy, E_a = 0.53 eV. The activation energy, E_a, thus obtained, is close to that obtained from high forward bias bulk resistance, R_s. In Fig. 3.10 all the points fit beautifully to the expression $R_s(T) = R_0 \exp(E_a/kT)$. The temperature dependence of I_g points to its origin from carrier recombinations in the depletion region. Rate of carrier recombinations increase with temperature due to increase in capture cross section. The change in the parameter E_0 with temperature implies that the leakge current I_t is due to thermionic-field emission tunnelling. For thermionic-field emission tunnelling, I_t actually becomes a complicated function of temperature, bias, barrier height and semiconductor parameters. Almost constant value of n over the temperature range 298 K to 397 K implies that the temperature dependent nonlinear process has been covered by the temperature dependence of I_g, I_t, and E_0. High n at low temperature (269 K) can attributed to field assisted processes such as, field emission tunnelling, hopping etc. A small

Table 3.1. Summary of results obtained from simulation.

T K	I_s(A)	Rs (Ω)	n	I_g(A)	I_t(A)	E_o(eV)
269	8.60×10^{-14}	3.62×10^{6}	1.48	8.20×10^{-15}	7.2×10^{-15}	0.033
282	2.10×10^{-13}	5.58×10^{5}	1.27	8.30×10^{-14}	2.1×10^{-14}	0.030
298	1.53×10^{-12}	2.59×10^{5}	1.27	1.29×10^{-12}	6.6×10^{-13}	0.034
324	2.45×10^{-11}	4.65×10^{4}	1.26	1.46×10^{-11}	8.1×10^{-12}	0.037
347	1.71×10^{-10}	1.42×10^{4}	1.26	9.67×10^{-11}	4.1×10^{-11}	0.038
371	1.09×10^{-09}	4.59×10^{3}	1.25	5.62×10^{-10}	2.2×10^{-10}	0.039
397	6.14×10^{-09}	1.61×10^{3}	1.25	2.50×10^{-09}	9.6×10^{-10}	0.041
417	3.29×10^{-08}	6.94×10^{2}	1.33	3.11×10^{-08}	1.8×10^{-09}	0.041

Table 3.2. Results of barrier height and activation energy obtained from various technique (DT indicates diffusion theory, TET indicates thermionic emission theory)

	From direct I-V Plot (eV)	From Simulation (eV)	From IPE (eV)
ϕ_b (DT)	0.82	0.89	0.92±0.02
ϕ_b (TET)	0.76	0.82	
E_a	0.51	0.53	.....

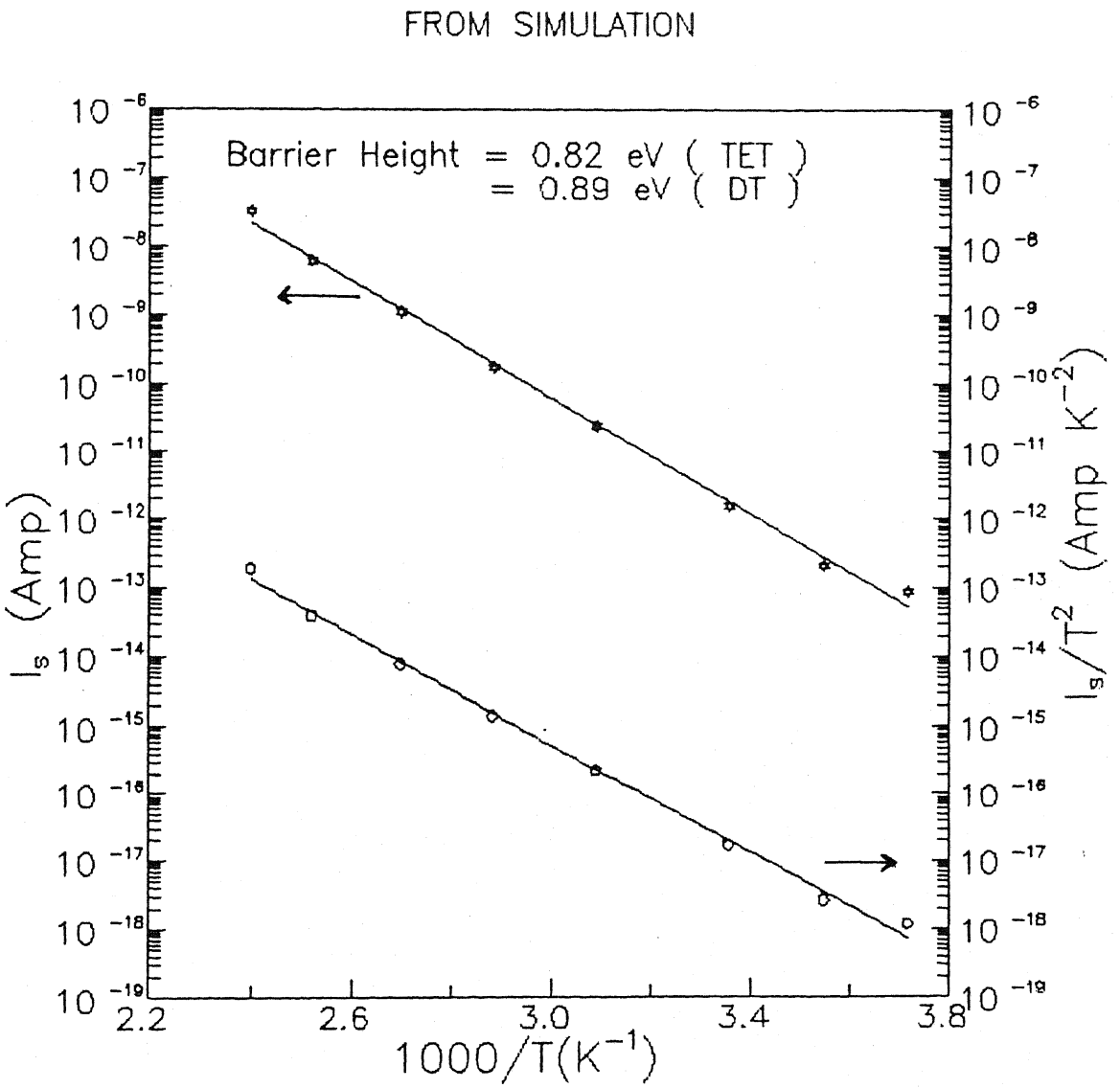

Fig. 3.9. The simulated value of saturation currents (I_s) plotted in both thermionic emission theory (circles) and diffusion theory stars).

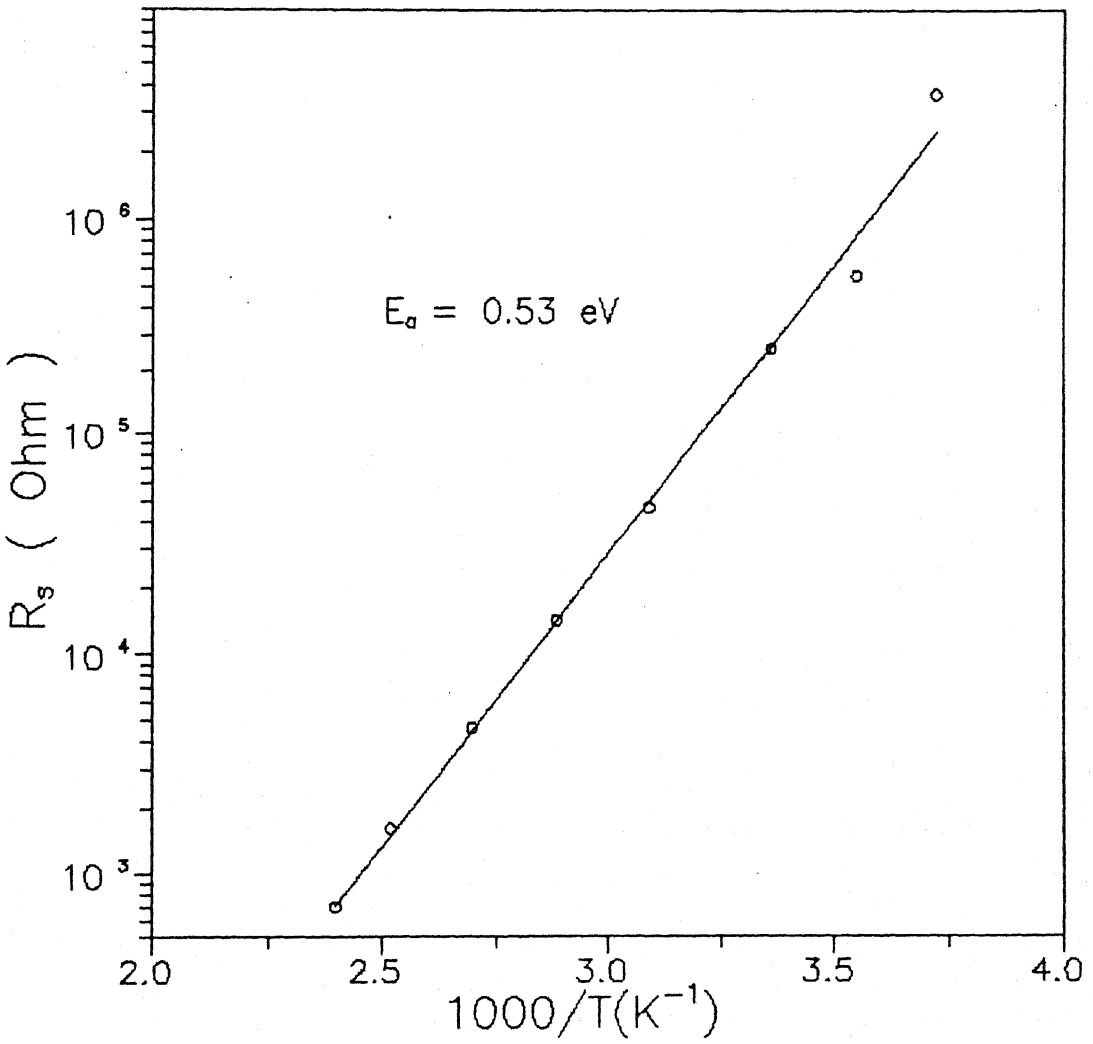

Fig. 3.10. The logarithm of simulated value of R_s plotted with the reciprocal of temperature (T).

increase in n at highest measuring temperature seems anomalous. It could be attributed to experimental errors.

We, therefore, can see that the computer modeling, after taking into account the established processes, offers good Schottky parameters , and at the same time implies that some more nonlinear processes other than recombination and tunnelling may be present as discussed in next discussion section.

3.3 Internal Photo Emission (IPE):

3.3.1 Theory of IPE:

Internal photo emission (IPE) is a component of the photo response of the diode. Several optical transitions can contribute to the photo response as shown in Fig. 3.11. Here 'A' represents the IPE in which light is absorbed in the metal and the electron is photoemitted into the a-Si:H. With the diode under reverse bias the electron transits the a-Si:H and is collected at the back contact. The IPE, as shown in fig. 3.11, turns on at energies less than the band to band absorption. Since the electron mean free path (mfp) in metal is small (~ 30 Å), it is necessary to illuminate the metal near the interface. For photons with energy greater than bandgap, and when significant light intensity exists in the a-Si:H, optical band to band absorption will occur. Since these carriers are excited into the extended states, they will be collected and contribute to the photo response. This process is represented by 'B'.

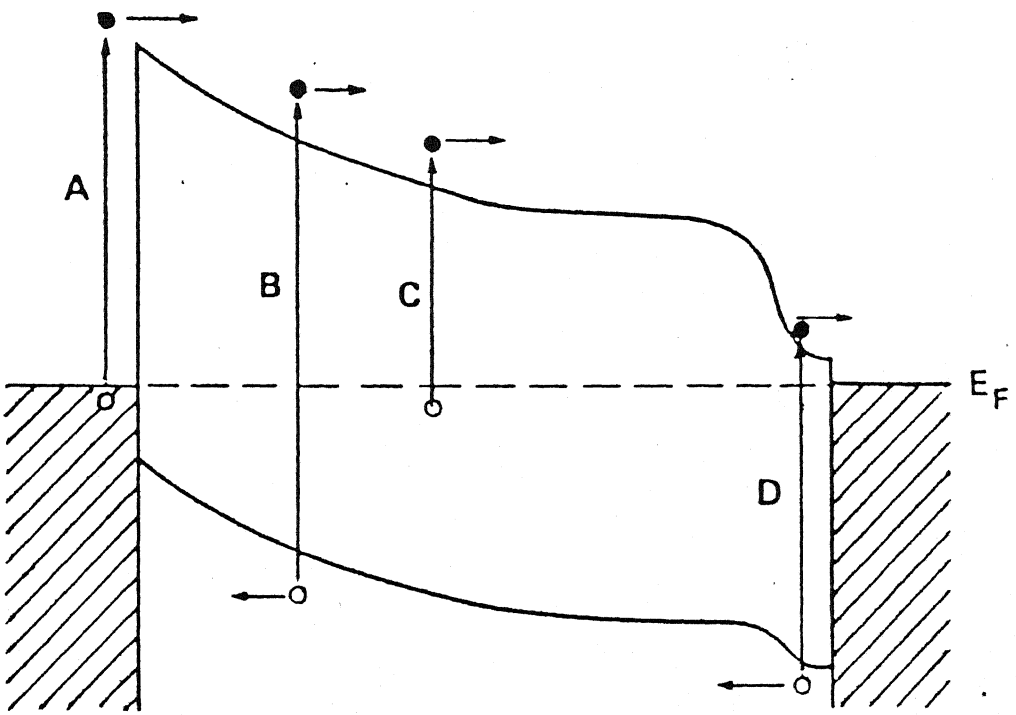

Fig. 3.11. A schematic of the optical transitions that contribute to the photoresponse of a-Si:H Schottky diodes. (a) internal photoemission; (b) optical band-to-band transition; (C) localized to extended state absorption; and (D) absorption in the doped layer.

There is subgap absorption indicated by process 'C', which may contribute to the photo response and mask the IPE. Here 'C' is a transition from occupied localized states below Fermi level to unoccupied extended states and 'D' is a transition in the heavily doped back contact region. Since transition 'C', observed in optical absorption spectra, occurs in the same energy region as the IPE, it might become difficult to distinguish IPE current from the subgap photoconduction current. The transitions in the heavily doped back contact involve extended states, and their (electron and hole) collection is more probable than the transitions involving localized states. But in order to contribute to photocurrent, the hole must transit the sample before its recombination. Since hole mobilities are lower, recombination with photoemitted electrons is likely, and so transition D will be suppressed.

The theory of IPE was originally worked out by Fowler. The photo emission yield (Y) per incident photon exhibits a wavelength dependence described by[7]

$$\left.\begin{aligned} Y(h\nu) &= B\,(h\nu - \phi_b)^2 \quad \text{for } h\nu > \phi_b \\ &= 0 \quad \text{for } h\nu < \phi_b \end{aligned}\right\} \quad \ldots\ldots\ldots (8)$$

where B is a constant determined by absorption of the metal and the probability of photoemission into the semiconductor. Thus the extrapolation of the plot $Y^{1/2}$ vs photon energy (E) —— known as Fowler plot, to Y = 0, will give the barrier height ϕ_b. The first

IPE results for a-Si:H Schottky barriers were reported by Wronski *et al*[41] in 1980. Their spectrum illustrated in Fig. 3.12 has two components: the strong absorption at E > 1.4 eV due to band to band transitions (process B) and weaker feature at E < 1.4 eV due to IPE (also sub gap to extended band adsorptions, process C). They had got $Y^{1/2}$ vs E plot as a straight line for Cr and Pd. But Nemanich *et al* [42] did not get a good straight line fit to IPE data on well characterized Pt/a-Si:H samples. Because of the high barrier of their Pt/a-Si:H junction, IPE did not turn on until near the band to band transitions, which along with other transitions tends to make the analysis more difficult. Some time, in fact, $Y^{1/3}$ dependence[43] might be found instead of $Y^{1/2}$. This dependence is expected for a thin oxide or insulator film between the materials (M/S). It should be noted that ϕ_b obtained from I-V measurements results in the zero temperature limit, whereas the IPE determines ϕ_b at the measured temperature. It has been found that the IPE measurement is independent of temperature[41]. Although there might have remained controversy over whether the measurements indeed represented IPE, a recent study on IPE of electrons as well as holes by Wronski *et al*[32,44], where they have also found mobility gap (~ 1.89 eV at room temperature) of a-Si:H using Pt, Pd and Ni/a-Si:H diodes, conclusively establishes the IPE process in a-Si:H. Fig. 3.13. shows the Fowler plot for their measurements.

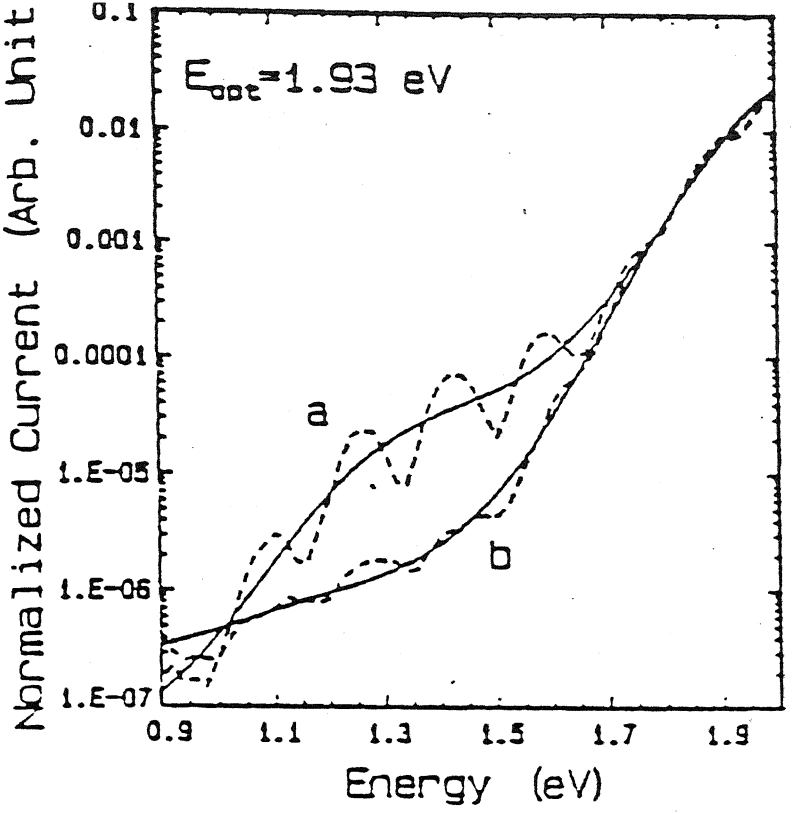

Fig. 3.12. Photoresponse of a-Si:H Schottky diodes under (a) forward bias and (b) reverse bias.
[from Hich *et al*[32]]

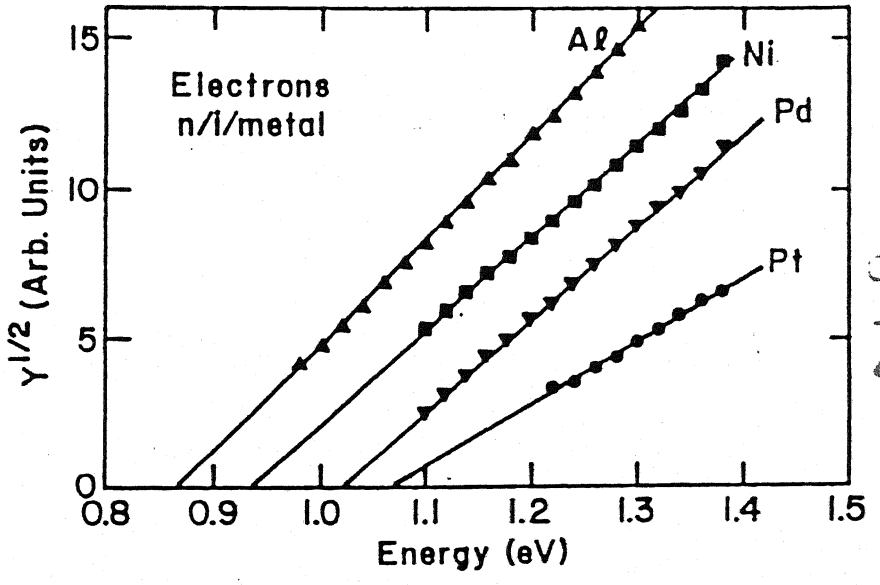

Fig. 3.13. Fowler plot for the internal photoemission of electrons into intrinsic a-Si:H.
[from Wronski *et al*[44]]

3.3.2 IPE Results:

A normalized photo response (or yield, Y) vs. photo energy (E) is plotted in Fig. 3.14 on log-normal graph scale for all biases. This figure shows three different absorption regions: the region, for E >1.7 eV is marked by A and corresponds to band to band transitions (process B). In this region photo energy (E) becomes too high relative to band to band absorption and hence photo absorption goes to saturation for E > 1.8 as shown in Fig. 3.14. The linear portion, B, indicates strong absorption for photo energy 1.7 > E > 1.4 eV, but decreases as E decreases. This is because the photon absorption takes place due to localized band tail states to extented states transitions and as photon energy decreases number of states avilable in band tail reduces. Taking exponential band tail the slope of linear portion of log(Y) vs E plot gives us the conduction band tail parameter as 27 meV. The third and all important C represents weak absorption for photo energy E < 1.4 eV. In this region IPE occurs, some subgap absorption may also be present where energy equals the barrier height. In this region Fowler plot, $(Y^{1/2} - E)$ shown in Fig. 3.15 results in ϕ_b as 0.92 ± 0.02 eV.

The log(Y) vs E plot for forward bias (V_f = + 1.0 V) along with zero bias is demonstrated in Fig. 3.16. Unlike Fig. 3.12 no interference fringe appeared here. This is because of high sample thickness ($\approx$ 4 μm). As seen from Fig. 3.16, in IPE region the

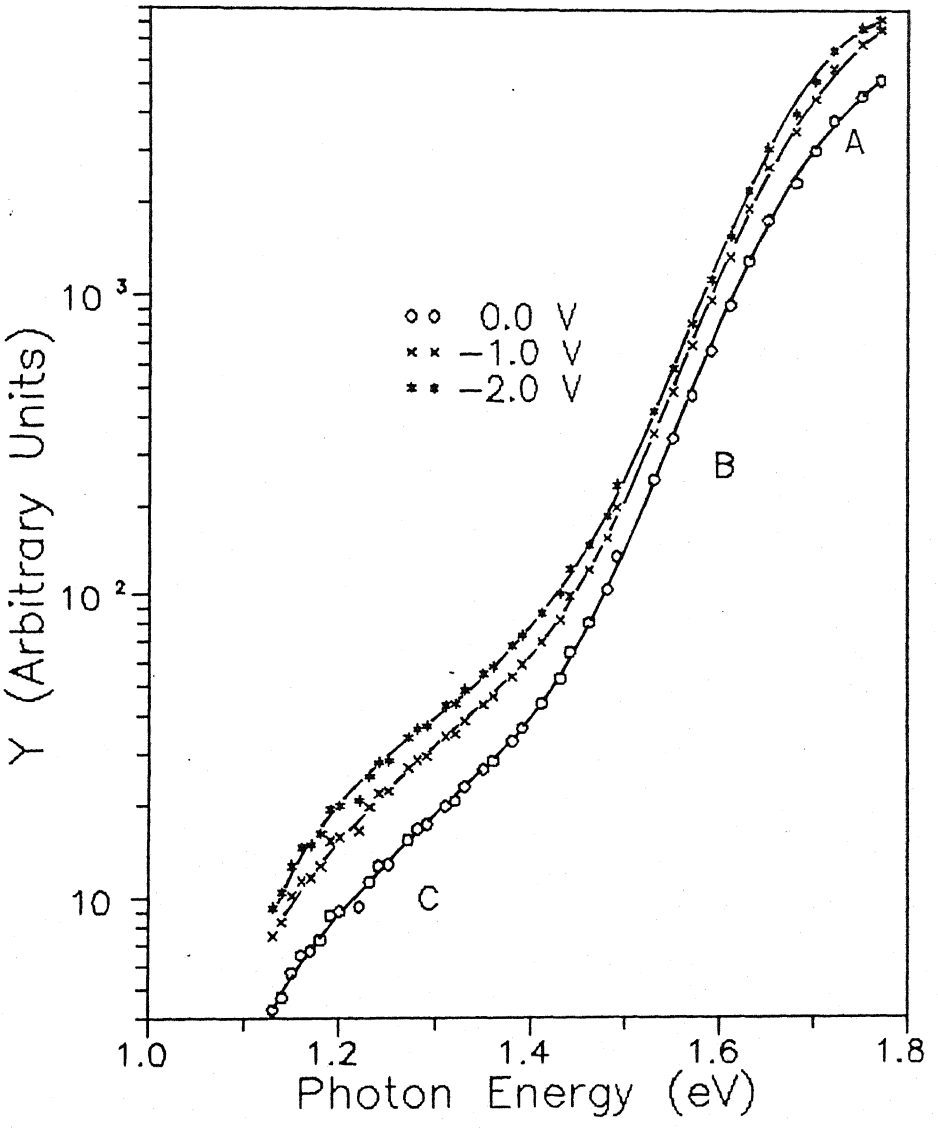

Fig. 3.14. Measured normalized photoresponse plotted with photon energy as a function of applied reverse bias across the Au/a-Si:H junction.

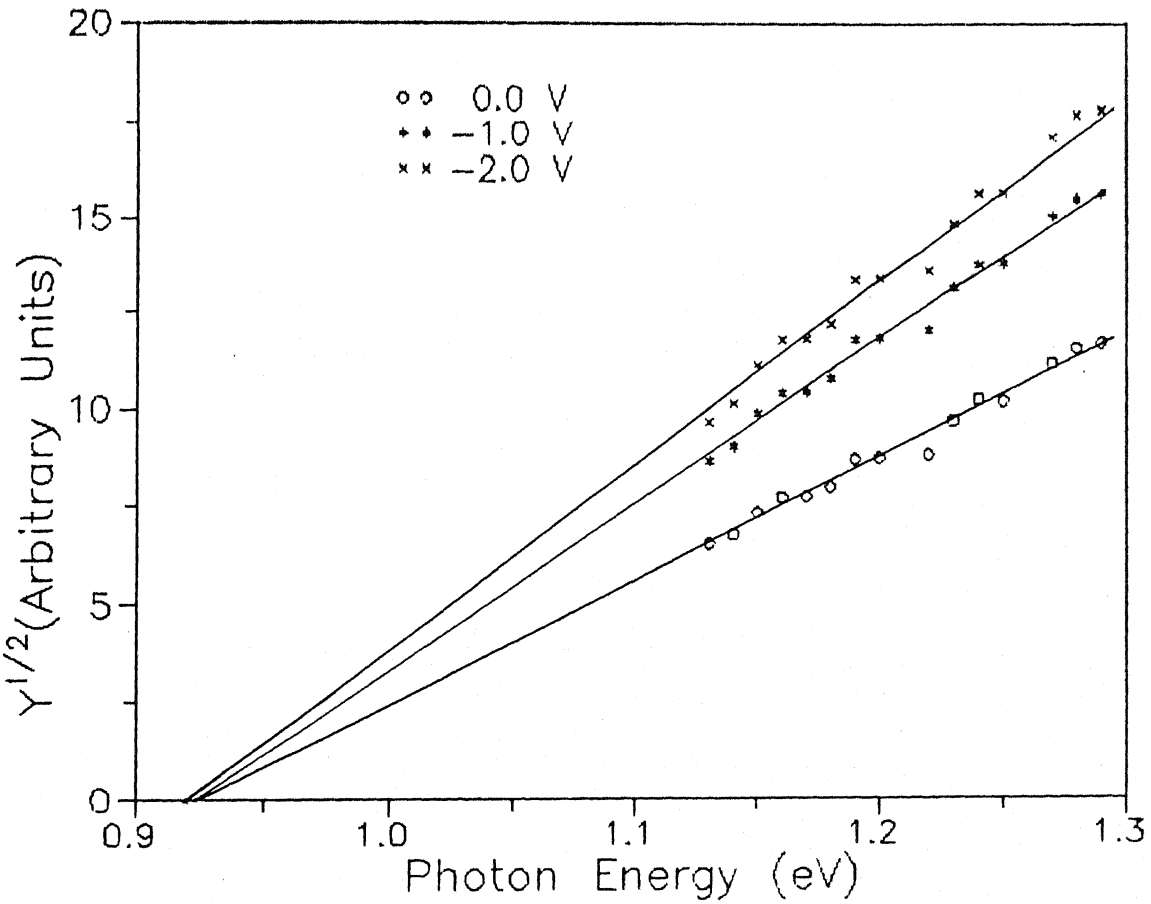

Fig. 3.15. Fowler plots as a function of reverse bias applied to the Au/a-Si:H Schottky barrier. Also shown its field dependence.

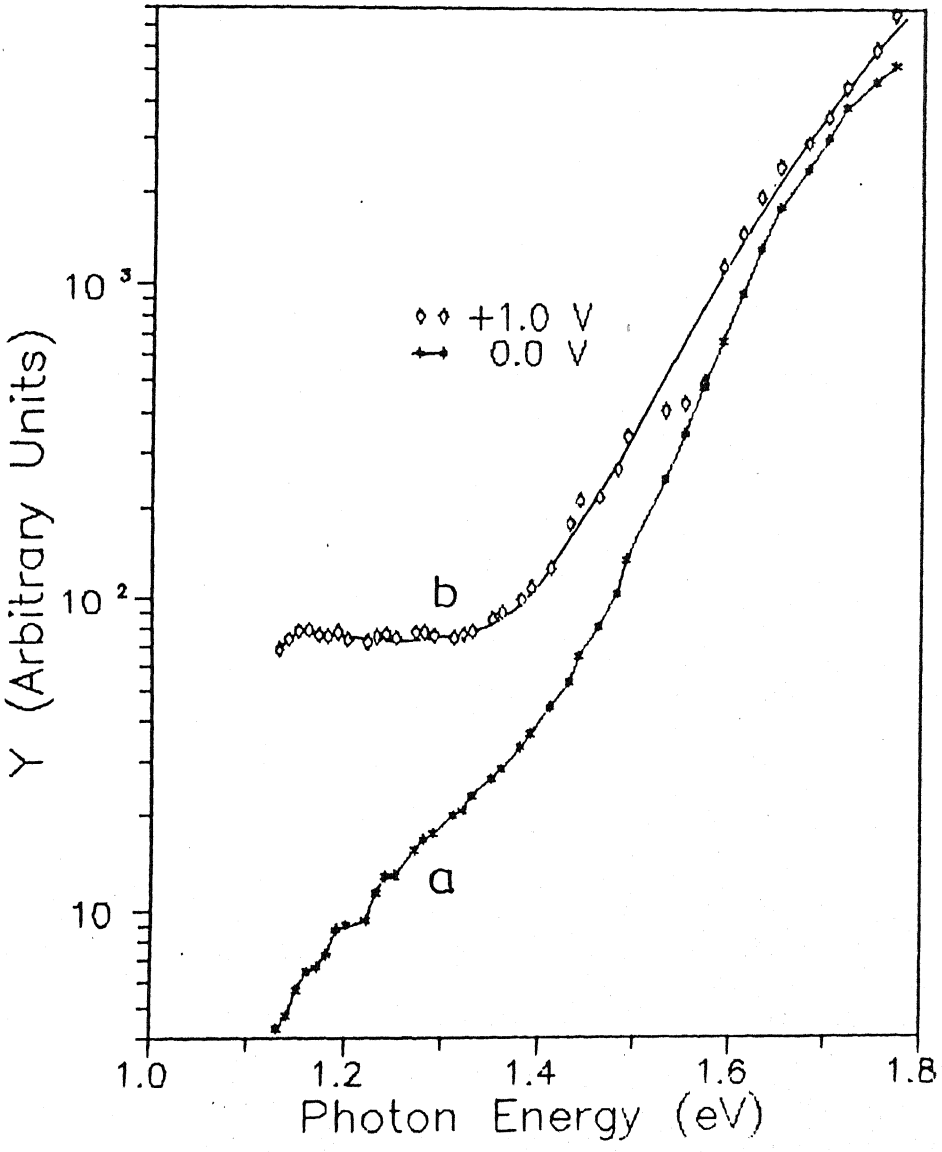

Fig. 3.16. Measured normalized photoresponse of Au/a-Si:H Schottky diode under (a) reverse bias 1 volt and (b) forward bias 1 volt.

photoresponse curve for V=+1.0 V remains almost constant. This can be attributed to large dark forward current and relatively weak photon absorption. This could have been overcome by taking IPE measurements using a light chopper.

3.4 Discussions on I-V, Simulations, and IPE Results:

So far in the previous three sections we have presented the details of results obtained by different techniques. First of all the results obtained at room temperature (Fig. 3.1) show very good rectification properties, which demonstrate the good quality of Schottky barrier diodes. This has also been reflected throughout the temperature range of measurement (269 K $\leq$ T $\leq$ 417 K) (Fig. 3.3 and 3.4). The diode parameters, n and I_s, are of significant importance. They may imply different carrier transport processes in Schottky barrier diode. The diode ideality factor, n, is 1.27 for dark I-V and 1.10 for I_{sc}-V_{oc} measurements at room temperature. This discrepancy in n has been attributed to the bulk series resistance of the diode because I_{sc}-V_{oc} measurements automatically exclude the bulk resistance effect. While in the other case series resistance effects alter the I-V characteristics by reducing the applied bias voltage across the barrier by an amount IR_s. Had R_s only been responsible for this difference in n, we would have expected the equation (1) (or (2)) to fit I_{sc}-V_{oc} data except when V is replaced by $(V-IR_s)$. In fact, this works in

case of crystalline Schottky barriers. But our results show that it is not true for amorphous Schottky barriers. In Fig. 3.2 one can see that at low forward bias, where effects of R_s are completely ignorable, dark I-V and photo I-V characteristics did not coincide. This implies the presence of some additive effects, which may not be present in I_{sc}-V_{oc} characteristics, besides series resistance effect. These effects contribute to the increase in the value if I_s and thereby increase n in order to fit the equation (2). Therefore, saturation currents derived from the straight line fitting of ln(I)-V plots lead to significantly incorrect value of barrier height. It generally results in a smaller value of ϕ_b. Hence it is necessary to separate the above mentioned additive currents along with the bulk resistance effect from I-V measurement. Further they make the fit to equation (1) or (2) worse at higher bias voltages where they become more predominant. Taking these into account theoretical fit to experimental data improves and one obtains the barrier height from these.Fig. 3.6 and 3.7 exhibit more or less good match between the computed best fit and experimental curves. Also, the diode parameters derived from simulation method are more reliable than those obtained from simple I-V plots. The value of ϕ_b from this simple technique is higher and more accurate compared to I-V plot. Again, I_s (from simulation) = $1.53X10^{-12}$Amp and I_s (from I_{sc}-V_{oc})

= $1.50X10^{-12}$ Amp at room temperature. This implies that results obtained from the simulation technique are more accurate and closer to actual values, since I_{sc}-V_{oc} measurements yield more accurate and reliable barrier height. But it should be noted that computed I-V curve exceeds the experimental I-V curve at higher biases (V >0.4 V). It happens over the whole temperature range (Fig. 3.7 & 3.8). This is attributed to the bias dependence of series resistance, R_s, which tends to increase at higher biases. But our simulation technique has assumed R_s as constant over the bias range. So the value of R_s obtained through simulation is some average of its value over the bias range. Therefore the estimated value of R_s becomes less than the actual value of R_s at high forward bias where its effect is more predominant. Fig. 3.10 exhibits very good R_s vs 1/T fit to equation $R_s = R_0 \exp(E_a/kT)$ with E_a, activation energy, equal to 0.53 eV. Exactly the same value of E_a has been obtained from from high forward bias dark I-V data (Fig. 3.6). This might seem less than expected on coplanar structure, where depletion region is extended over the whole thickness of a-Si:H layer and quasi Fermi level for electrons moves upward (i.e., towards conduction band) throughout the bulk when Schottky junction is forward biased. We, therefore, get the activation energy as a difference between the extended band and quasi Fermi level. When the voltage across the sample is changed from V_1 to V_2 and corresponding current is changed from I_1 to I_2,

then the shift in quasi Fermi level (ΔE_{Fn})[45] can be given by

$$\Delta E_{Fn} = kT\ln(I_2V_1/I_1V_2)$$

$$\sim 0.28 \text{ eV} \quad [\text{for } V_1 = 0.1 \text{ V} \ \& \ V_2 = 1 \text{ V}, \ I_2/I_1 \sim 10^5 \text{ and } T = 300\text{K}]$$

So the activation energy corresponding to neutral bulk region is approximately (0.53 + 0.28) eV or 0.81 eV. Moreover Schottky junction properties are very much sensitive to the metal used in contact. It has been reported by numerous groups[46] that E_a differs in two Schottky barriers on the same a-Si:H but with different metals. The activation energy is also dependent on structure as well as its preparation technique. Therefore, activation energy in neutral bulk region of a-Si:H is expected to be different from the active Schottky structure. We now consider the decisive results of internal photoemission (IPE) on the very same diode (#4). Fig. 3.14 demonstrates the feature of IPE similar to that reported in Fig. 3.12. The band tail parameter (E_0) is calculated from the slope of the linear portion of log(Y) vs E plots, assuming the exponential relation ~ exp(-E/E_0). The value of E_0 obtained is 27 meV. Therefore it conclusively establishes the occurrence of IPE in our Schottky diodes. Fig. 3.15 gives us the Schottky barrier height, ϕ_b as 0.92 eV at zero bias. It also clearly illustrates the dependence of ϕ_b on reverse bias. This bias dependence of ϕ_b arises from the image force lowering effect as discussed in Chapter I. Recalling the results of dark I-V characteristics, we

note two interesting facts simultaneously. First, the value of ϕ_b, equal to 0.92 agrees well with barrier obtained from diffusion theory rather than thermionic emission theory. Therefore it automatically favours the diffusion theory. Second, it also demonstrates the validity of our simple simulation technique for better determination of Schottky barrier height and other associated diode parameters.

One may wonder as to why the simulated value of n instead of improving worsens a bit through simulation. But this can easily be explained if we view Fig. 3.17 carefully. In this figure, n obtained directly from the slope of dark I-V characteristics decreases considerably with increasing temperature whereas computed n remains constant over the wide range of temperatures except at very high and very low temperatures. The temperature dependent additive currents decrease n by straightening the dark ln(I)-V characteristics as their effects increase with temperature. Therefore, since simulation minimizes the temperature dependence of n by extracting I_g, I_t and E_0 out of dark I-V data, n is almost constant with temperature. But increased value of n at much below room temperature can be assigned to low temperature phenomena[47], such as hopping conduction, field-emission tunneling etc.

Thus we summarize the results and discussion by highlighting the following points:

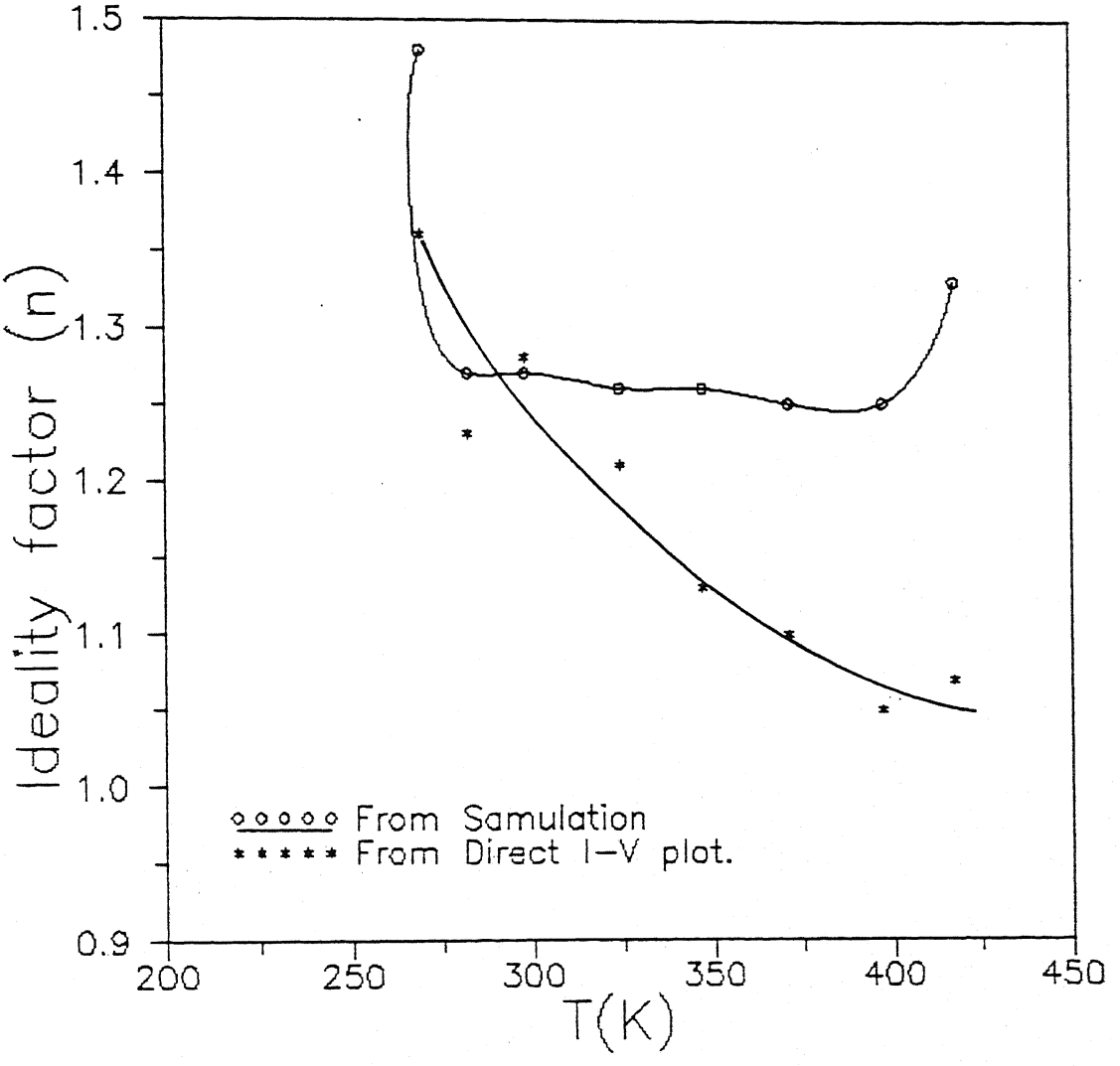

Fig. 3.17. A Plot of ideality factor (n) as a function of temprature (T)

1. Our Au Schottky diodes on undoped a-Si:H, have low n ($\leq$ 1.1) and high rectification ratio (> 10^5 at 2.0 V).

2. The saturation current, I_s, obtained from the dark I-V measurements under forward bias is not adequate to characterize the Schottky barrier. The saturation current (I_s) includes the effect of bulk resistance and leakage currents, and thereby increases the barrier height ϕ_b.

3. We show that a simple computer simulation does help. Moreover it also provides insight into carrier transport and related phenomena, such as strong bias dependence of bulk resistance.

4. The saturation currents obtained directly from the extrapolation of dark I-V characteristics as well as from simulation, fit equally well to both thermionic emission theory and diffusion theory. It is shown that forward bias dark I-V characteristics cannot distinguish between these two carrier transport mechanisms over a-Si:H Schottky barriers.

5. However, it is found that the results of Internal photoemission (IPE) favour diffusion theory for carrier transport over the Schottky barriers. The ϕ_b obtained from IPE measurements agrees well, within experimental error, with that obtained from our simple model from computer simulation, using diffusion theory.

CHAPTER IV

CAPACITANCE AND CONDUCTANCE MEASUREMENTS

While the current-voltage (I-V) characteristics of an amorphous silicon diode exhibit properties more or less similar to those of crystalline silicon, the capacitance properties are distinctly different. A commonly used measurement for characterizing Schottky barrier on crystalline silicon is capacitance-voltage (C-V), where standard plotting $1/C^2$ versus V is used to obtain the built-in potential, V_d, from the intercept to the voltage axis. Because of the large concentration of deep localized states in the gap this standard analysis does not work in a-Si:H case. The analysis of C-V data is dependent on the gap states densities and hence the barrier profiles. Hence the measurement of density of localized gap states or simply density of state (DOS) in the gap has attracted the attention from the beginning of this field of science and technology.

But our motivation is not so much the estimation of DOS in the gap as consistent interpretation of ac measurements on the same sample. In this chapter we describe the results and its interpretation of ac response obtained from simultaneous measurements of capacitance and conductance as a function of both frequency and bias. By analyzing these data at varying bias, one can, in principle, study both the spatial and energy dependence of

DOS. The spatial variation particularly close to the interfaces can be studied on going down to very low frequency measurements. Thus through capacitance and conductance measurements one can obtain information regarding both the interface and bulk properties. It is found that dc and ac measurements on the same Schottky barrier do give consistent results.

4.1 Theory:

The formation of Schottky barrier on crystalline semiconductors is well established. However, transferring similar ideas to the situation of amorphous materials is quite complicated due to the presence of large density of states (DOS) in the gap. Nevertheless, it can be used, at least for undoped amorphous semiconductors with no loss of validity except that the role of the dopants is taken over by the presence of localized states in the barrier region. At thermal equilibrium, these localized states in the bulk are considered electrically neutral when the states above the Fermi level are filled and the states below the Fermi level are empty. Towards the metal/a-Si:H interface, Fermi level lies deeper in the gap with respect to conduction band edge as bending occurs upwards. As a result some of the states which are below Fermi level in the bulk, now lie above it in the interfacial region. At thermal equilibrium all states above the Fermi level are empty and hence are charged thereby giving rise to a space

charge in the barrier region. Fig. 1.2d shows a schematic of energy band diagram for a metal/a-Si:H Schottky barrier. In the space charge region the bands bend resulting in spatial variation of barrier potential (V(x)), which has a maximum at the metal/a-Si:H interface.

Consider now the ac response of a Schottky barrier diode. Fig.4.1 is drawn for the ac half cycle in which the metal is connected to negative bias. The electrons are released from deep states at A in the barrier region (depletion region) and transferred to the Fermi level, E_F, in the back contact. As modeled by Gibb and Long[1] this process can be considered as a two stage process: the first involving the transfer of electron to a band state at the edge of the Schottky barrier at B; and the second involving the drift to the back contact and de-excitation. The stage-I has been treated using the standard perturbed rate-equilibrium method leading to a Debye response for the process of the form $[1+i\omega\tau]^{-1}$, where ω is the angular frequency of the signal, i is $\sqrt{-1}$, and τ is the relaxation time given in terms of the relaxation rates for the process A $\longrightarrow$ B and B $\longrightarrow$ A by

$$\tau^{-1} = \omega_{ab} + \omega_{ba} \qquad (4.1)$$

The contribution of the state A to the charge released from the barrier as a function of ω depends, therefore on the real part of the Debye response, i.e, on $[1+\omega^2\tau^2]^{-1}$. The rate determining term

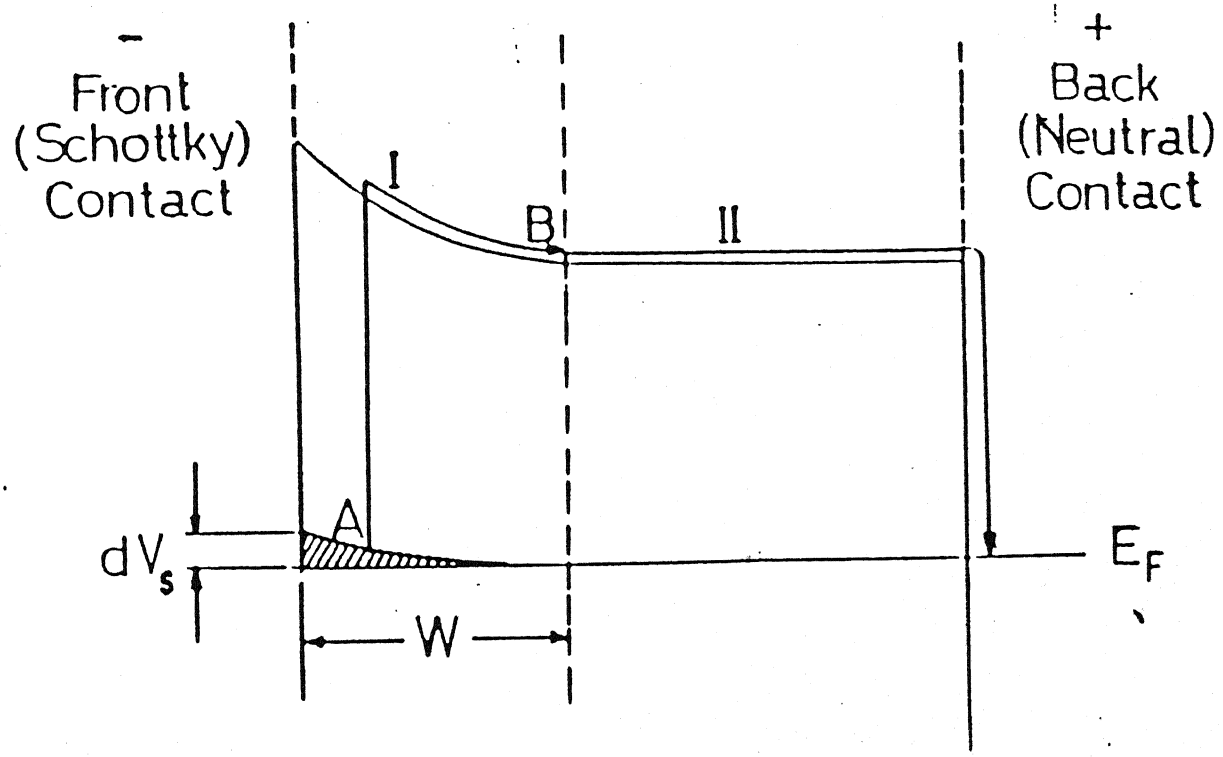

Fig. 4.1. Deep state trap release under (reverse) perturbing bias dV_s zero dc bias.

τ will be that involving thermal excitation of the electron into the conduction band (E_c). Due to the barrier profile as shown in Fig. 4.1, this rate will vary with position and hence $\tau(x)$ at x from metal/a-Si:H interface can be given in the following form:

$$\tau(x)=\tau_0 \exp[(E_c-E_F+qV(x))/kT] \quad \ldots\ldots \quad (4.2)$$

where τ_0 is an empirical rate parameter (equivalent to lattice vibration rate in crystalline solids).

In order to calculate the over all response, assumptions about DOS in the Schottky region have to be made. To start with, taking a DOS at Fermi level (N_F) as uniform in both space and energy, and with the assumption that Schottky barrier is determined by the deep states, V(x) can be directly written, from Poission equation, as

$$V(x) = V_s \exp(-x/L) \qquad (4.3)$$

where

$$L = (1/q)(\varepsilon/N_F)^{1/2} \qquad (4.4)$$

with ε being the static permittivity of a-Si:H and V_s the barrier potential at metal/a-Si:H interface.

L is called the Debye length or screening length in the a-Si:H. When an ac signal is applied, V_s will change by an amount dV_s. Assuming that the perturbation voltage follows the same functional relation as the internal bias voltage, the change in

V(x) at x in the depletion region becomes

$$dV(x) = dV_s \exp(-x/L) \qquad (4.5)$$

With this change Fermi level will be lowered (or raised) and the charge density $\rho(x)$ will be increased (or decreased) by $d\rho(x)$. By lowering (or raising) Fermi level, the electronic states are vacated (or filled), thus creating (or reducing) the amount of space charge. The number of states vacated (or filled) equals the increase (or reduction) in the charge, so

$$d\rho(x) = qN_F[qdV(x)] = q^2 N_F dV(x) \qquad (4.6)$$

Using equations (4.3) - (4.6) we can calculate the charge dQ introduced or removed from the barrier by the potential change dV_s, and if C_s and G_s are the differential barrier capacitance and its parallel conductance at particular ω, then it becomes straight forward that

$$C_s(\omega) - i G_s(\omega)/\omega = \frac{dQ\omega)}{dV_s} = \int_0^\infty [N_F q^2 \exp(-x/L) \frac{dx}{1+i\omega\tau(x)}] \qquad (4.7)$$

Separating real and imaginary parts we can get

$$C_s(\omega) = \int_0^\infty (N\ q_F \exp(-x/L) \frac{dx}{[1+\omega^2\tau^2(x)]})$$

$$\text{or } C_s(\omega) = C_0 \left[1 - \frac{kT}{2qV_s} \ln\left(\frac{1+(\omega\tau'')^2}{1+(\omega\tau')^2} \right) \right] \quad \ldots\ldots(4.8)$$

and

$$G_s(\omega) = \omega^2 C_0 \int^{\infty} \left(q^2 N_F \exp(-x/L) \frac{\tau(x)dx}{[1+\omega^2\tau^2(x)]} \right)$$

$$= C_0 \omega \frac{kT}{qV_s} [\tan^{-1}(\omega\tau'') - \tan^{-1}(\omega\tau')] \quad \ldots(4.9)$$

where
$$\left.\begin{aligned} C_0 &= q^2 N_F L = \varepsilon/L; \\ \tau_0' &= \tau_0 \exp[(E_c - E_F)/kT]; \\ \tau_0'' &= \tau_0 \exp[(E_c - E_F + qV_s)/kT] \\ &= \tau_0' \exp[qV_s/kT] \end{aligned}\right\} \quad \ldots\ldots\ldots\ldots\ldots\ldots(4.10)$$

Here and throughout this work capacitances and conductances are expressed per unit area. Fig. 4.2 shows the general shape of C_s when plotted as a function of $\ln(\omega)$ at various T and V_s. As evident from the equation (4.8) C_s tends to C_0 at low frequency and C_s tends to 0 at high frequency. At intermediate frequencies there is a region of linear dependence which, if plotted to frequency axis, has an intercept value τ_0'. The shift in intercept at C_s=0 with T can be found from bulk activation energy.

All the above calculations have been done for zero dc bias. However, these calculations can be extended to describe the situation where dc bias is applied to the barrier, if the following conditions are satisfied:

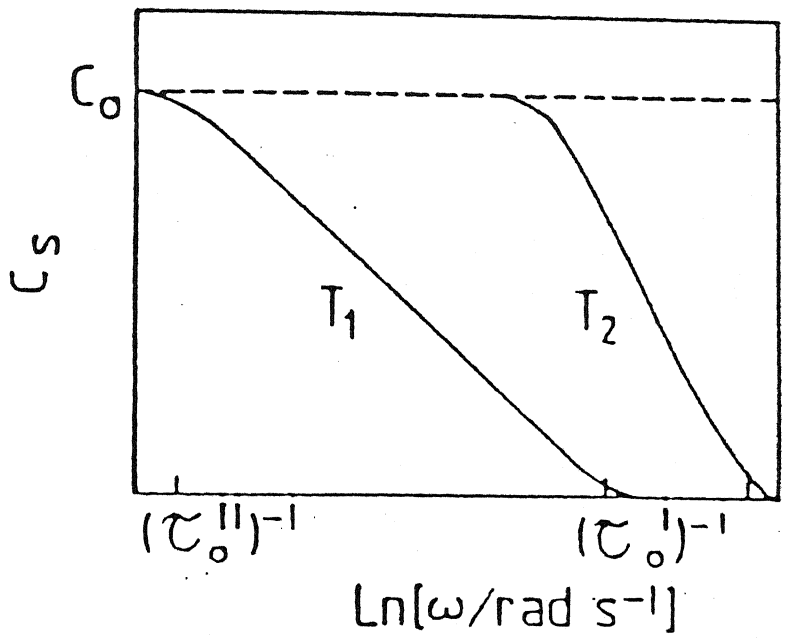

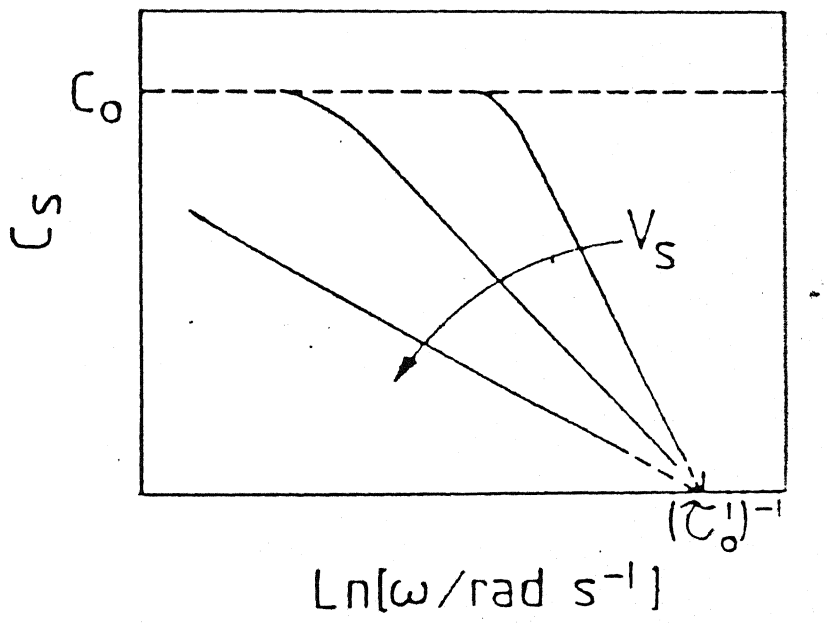

Fig. 4.2. Simplified theoretical variation of Schottky barrier differential capacitance with frequency: (a) for different temperatures; (b) for different interface potentials.

(i) that the surface state density is negligible;

(ii) that the electron quasi-Fermi level is flat throughout the barrier region; and

(iii) that the occupancy of the localized states is determined by the electron quasi-Fermi level.

And then only we can expect the diode behaviour shown in Fig.4.2b, where all the bias curves extrapolate to the same intercept frequency, since τ_0' does not depend on V_s.

Actually the assumption that for constant N(E) the perturbing signal follows the internal dc potential and drops of exponentially over the Debye length is true only at very lo frequencies, where states can all respond to the applie potential; at frequencies greater than $(\tau_0'')^{-1}$ it is necessary t make a more complex equation not readily solved. However, as a initial approach, we can use the abrupt cut-off model of Spear e al [48], where the states having relaxation time greater than ω^{-1} are assumed not to respond to the signal potential, whereas the states with relaxation times less than ω^{-1} are taken to respond fully. As evident from equations (4.2) and (4.3) τ decreases monotonically with x; hence it is possible in the analysis to define critical position (d) in the film where $\omega\tau(d) = 1$. As a consequence, for x < d no states respond and for x>d every one does. This same concept is also used by Viktovitch and Moddel[49].

For complete solution by this cut-off model, it is necessary

to consider the back contact properties for finite sample thickness (d_0). We consider the neutral back contact with dc built-in potential identically zero at the interface. Then the equation (4.4) can be rewritten in the form:

$$V(x) = V_s \frac{\sinh[(d_0-x)/L]}{\sinh(d_0/L)} \quad \text{.....(4.11)}$$

On substitution of this equation (4.11) into equation (4.3), we can get the expression for d corresponding to frequency ω as

$$d(\omega) = d_0 - L \sinh^{-1}\left(\frac{kT}{qV_0} \sinh(d_0/L)[1-\ln(\omega\tau)]\right) \text{..(4.12)}$$

Hence, on solving exactly the Poission equation the differential capacitance takes the form:

$$C = C_o \frac{1}{[d/L + \tanh[(d_o-d)/L]]} \quad \text{.....(4.13)}$$

By examinig the equation (4.13) one can get the limiting capacitance as ε/d_0, the geometrical capacitance and C_0 at high and low frequencies. The equation (4.13) shows two discontinuities at $1/\tau_0'$ and $1/\tau_0''$ as evident from Fig. (4.3). These discontinuities are the direct result of using the abrupt cut-off model, and is obviously unphysical. Therefore it is not straight-forward to deduce the expression for the imaginary part of the response, i.e., the conductance. To over come these

difficulties, it has been suggested by Gibb and Long[46] to use, instead of analytic solution of equation (4.13), the approximation

$$C = C_g + C_s(\omega); \qquad G = G_s(\omega) \quad \ldots\ldots\ldots(4.14),$$

where C_g is the geometric capacitance. Here the saturation capacitance is used as $(1-L/d_0)C_0$ in place of the full C_0. The result of this approximation has been shown along with the exact calculation in Fig. 4.3. The close agreement gives the justification of approximation to the analytic form.

It should be noted that in all the previous calculations so far no effect of stage II (in Fig.4.1) has been included (since an electron emitted from a deep state has been assumed to travel directly to the back contact). To include its effects, a finite voltage drop necessary to drive the current through the bulk of the material can be assumed; and this can be done by putting a conductance G_{b0} in series with the barrier elements C_s and G_s. The current flowing over the barrier can also be taken into account by means of a conductance G_{s0} in parallel with G_s, so that dc resistance of the whole device is given the series combination of G_{b0} and G_{s0}.

At high frequency ($\omega > 1/\tau_0'$), where C equals C_g the charge is stored on the electrodes, and the film acts as a passive dielectric. On the other hand as ω drops below $1/\tau_0'$ and the deep states begin to contribute to the capacitance, the charge starts transferring to the back contact through G_{b0}. These suggest that

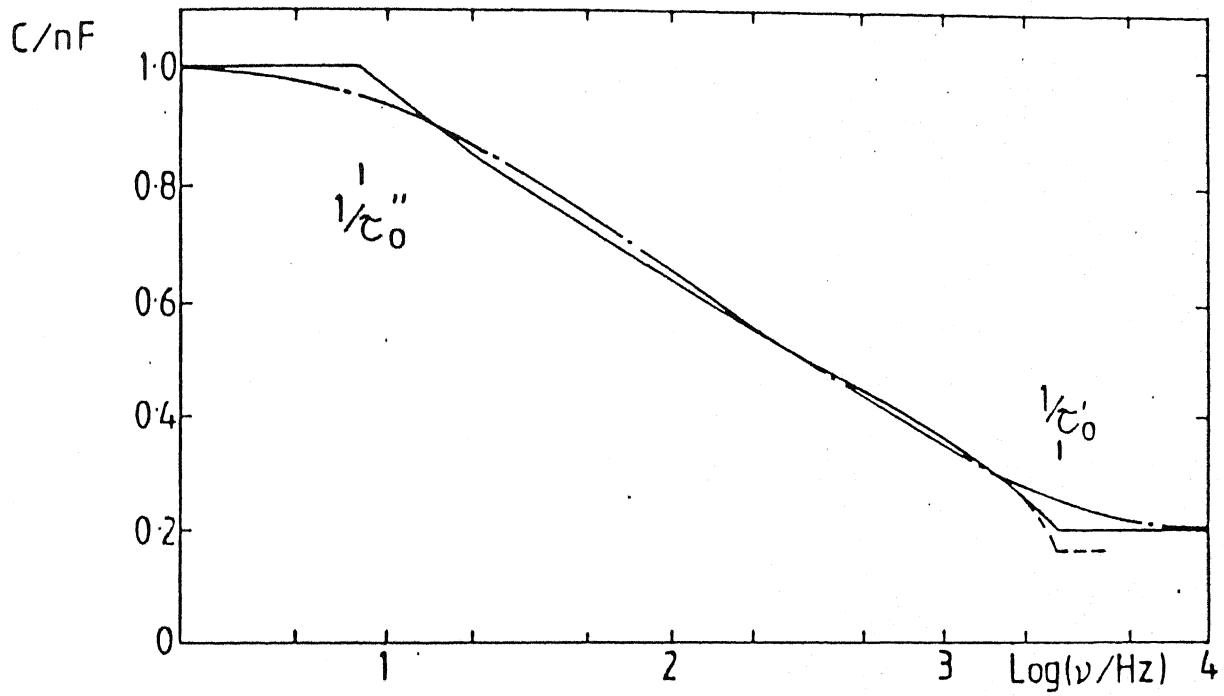

Fig. 4.3. Detailed models for capacitive response of the Schottky barrier: solid line → model of capacitance; dots → model of Viktorovitch and Moddel; dashes → approximation using equation (4·8) and the geometrical capacitance.

if equation (4.14) is used to represent capacitance, two elements C_s and C_g should be split up with only C_s in series with G_{bo}, thereby giving the ac equivalent circuit shown in Fig. 4.4. This equivalent circuit is accurate for frequencies $\omega \leq 1/\tau_o'$. But as the frequency drops the field is screened from the back contact by deep states in the Schottky barrier and the charge stored in the back contact drops below $V_s C_g$, making the above equivalent circuit inaccurate. This error becomes greater at low frequency when C tends to C_o because C will be underestimated by a factor $C_o L/d_o$.

An alternative circuit was modeled by Beichler et al[50]. But in order to get a capacitance, at high ω, of geometric value it is necessary to split C_g into two components representing Schottky and bulk region of the film respectively, with series combination being equal to C_g. And this splitting runs into trouble giving unphysical mechanism as discussed by Gibb and Long[46].

As we are being restricted to high frequency region, we used the equivalent circuit in Fig. 4.4, which represents the measured parameters in the form:

$$\left.\begin{aligned} G_m(\omega) &= \frac{[\,G_t G_{bo}(G_t + G_{bo}) + G_{bo}\omega^2 C_s^2\,]}{[\,\omega^2 C_s^2 + (G_t + G_{bo})^2\,]} \\ C_m(\omega) &= C_s G_{so}^2/[\,\omega^2 C_s^2 + (G_t + G_{bo})^2\,] + C_g \end{aligned}\right\} \quad \ldots.(4.15)$$

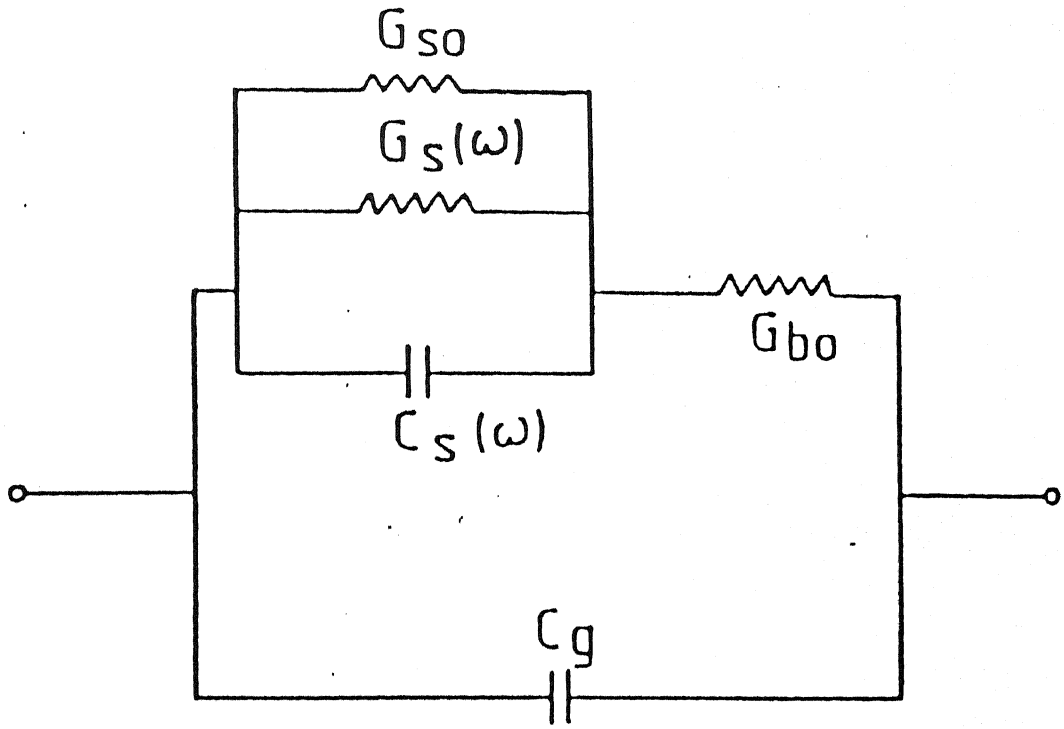

Fig. 4.4. Equivalent circuit (modeled by Gibb and Long) used in this work to model the sample behaviuor.

where $G_t = G_s(\omega) + G_{s0}$.

The value of C_g can be found from high frequency measurements, where $C_s(\omega)$ drops to negligible levels; G_{b0} may be approximated from Ohmic region (I-V) characteristics; and G_{s0} can be used as the static conductance of the sample. Then G_s and C_s can be derived on solving equations (4.15) and hence C_0 may be deduced from equation (4.7) to estimate N_F at different bias voltages.

4.2 C- V Measurements:

The capacitance (C) and conductance (G) of the sample were measured with HP Impedance Analyzer model 4194A as a function of frequency and dc bias. The dc bias voltage on the sample was applied from the inbuilt voltage source of the Impedance Analyzer, having frequency range from 100Hz to 15MHz. The oscillation level (i.e., the ac voltage drop across the sample) of the signal was maintained at 200 mV (r.m.s) thoughtout the measured frequency range. The contribution from the leads and the input impedance of the bridge were balanced out; and this balanced condition was stored in the bridge memory to keep it active throughtout the frequency and bias ranges. When dc bias of the sample was changed, it was allowed to relax for typically 15/20 minutes to allow any slow process to reach equilibrium before further measurements were made. Care was taken for proper grounding of the circuit elements, and to minimize the stray light effects. The static dark

capacitance and conductance, at different dc bias voltages, (-1.0V to 2.0V) were measured over frequency range 10^2 to 10^5 Hz.

4.3 Results and Discussions:

Fig. 4.5 shows the measured sample capacitance (C_m) as a function of frequency (ω) at different bias voltages., whereas the Fig. 4.6 illustrates the measured capacitance (C_m) as a function of bias voltage at different frequencies (ω). These two figures exhibit the expected qualitative behaviour. In Fig. 4.5 measured capacitance (C_m) at particular bias decreases monotonically with increasing frequency (ω) and all C_m vs $\ln(\omega)$ curves tend to converge to a particular value of C_m, which is independent of bias. This bias independent saturated value of measured capacitance (C_m) at higher frequencies is the geometrical capacitance (C_g) of the sample. This geometrical capacitance gives the sample thickness (d_o), using the relation: $d_o = \varepsilon / C_g$, as $\approx 7\mu m$.

It should be noted in Fig. 4.6 that the measured capacitance (C_m), for particular frequency (ω), remains almost constant, with little frequency dispersion, for reverse bias, but increases very sharply with forward bias and reaches its maximum values after which it decreases drastically with the further increase in forward bias to the geometrical capacitance (C_g) of the sample. Similar behaviour is also observed for other frequencies (in Fig. 4.6). The height of the peak in forward bias decreases with

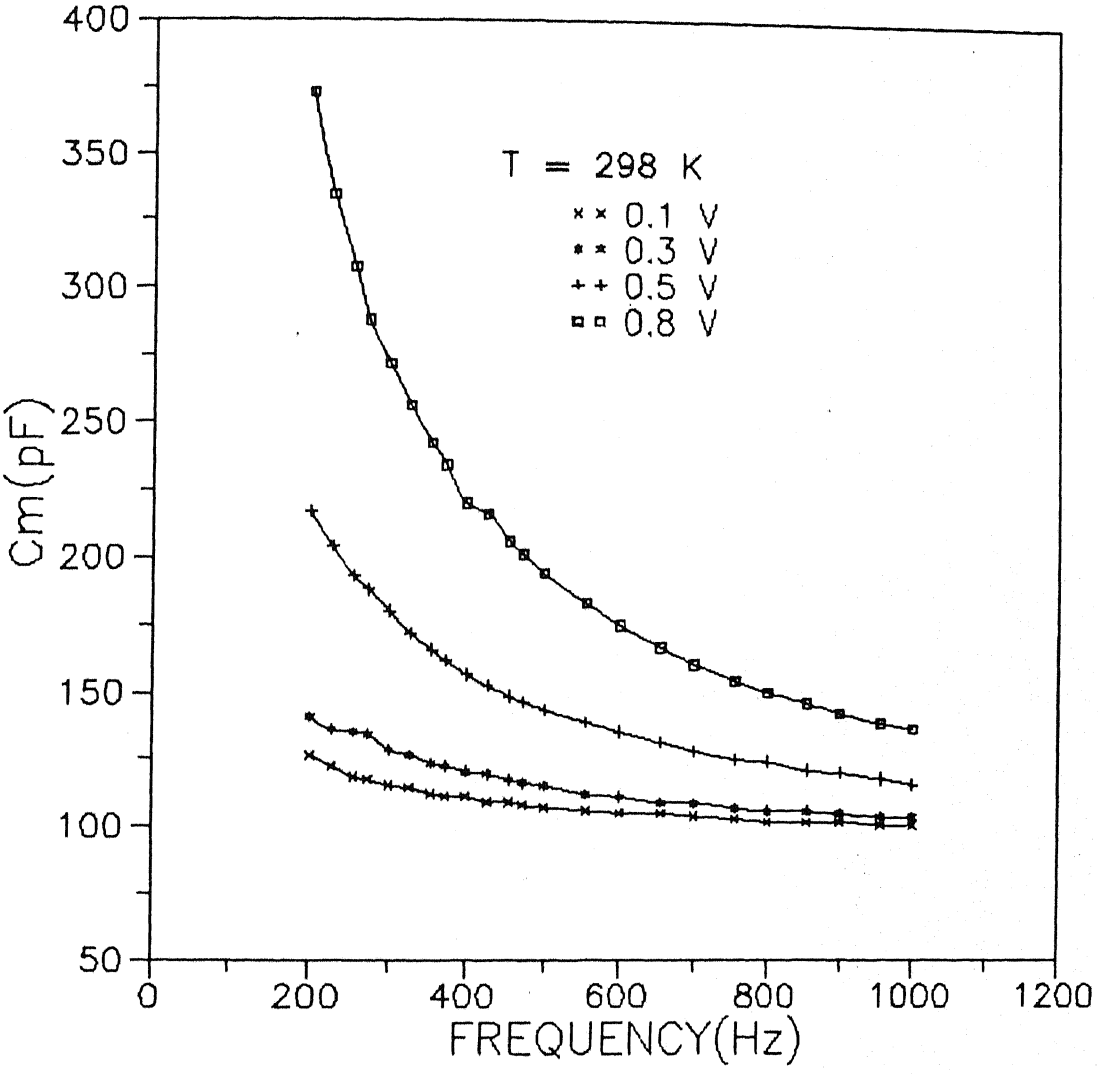

Fig. 4.5. Measured capacitance (C_m) and conductance (G_m) plotted as function of frequency at various applied dc bias voltages.

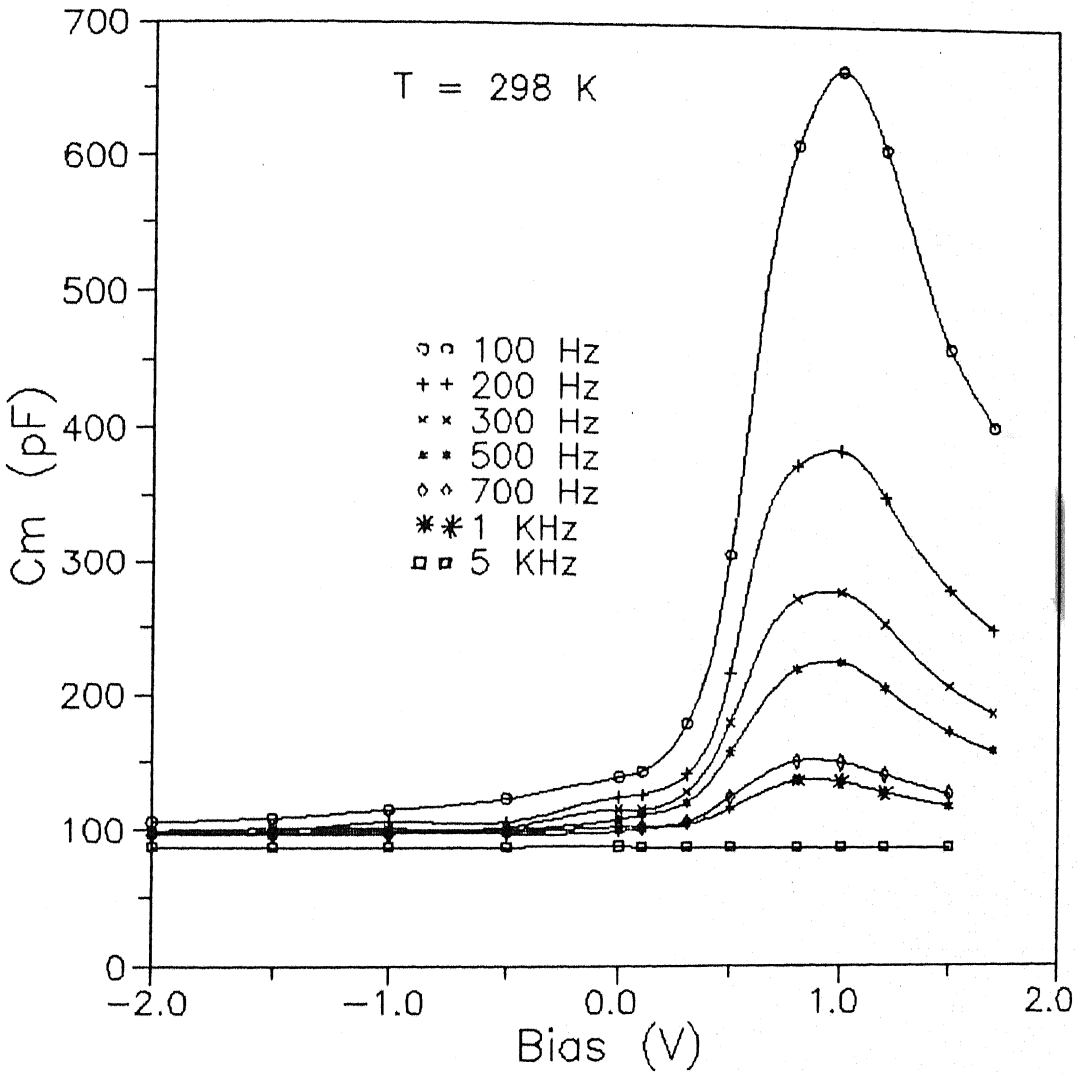

Fig. 4.6. Measured capacitance (C_m) versus dc bias applied to the Au/a-Si:H Schottky junction as a function of frequency. All C_m-V curves having maximum at ≈ 1.0 V.

increasing frequency and finally flattens at very high frequency ($\approx 10^3$). But the peak position of capacitance is around 1.0 V and it remains independent of frequency. Similar C_m vs V characteristics were also observed by others[51,52], who explained it as bulk series conductance effect. As forward bias increases, the Schottky resistance (i.e.,the junction resistance) decreases and gradually it approaches the bulk resistance. Thus when the Schottky conductance equals the bulk conductance the peaks in C_m vs V curves occur. With further increase in forward bias voltage, the bulk conductance dominates the processes making the junction a passive dielectric and hence reduces C_m to C_g, the geometrical capacitance of the sample.

The junction parameters (C_s & G_s) are deduced from the measured parameters (C_m & G_m) using the equations (4.15). In this procedure, C_g is taken from Fig. 4.5. The dc Schottky conductance (G_{s0}) and bulk conductance (G_{b0}) are derived from I-V measurements. The results of this procedure are illustrated in Fig. 4.7 for zero dc bias and in Fig. 4.8 and 4.9 for nonzero biases. These two figures show similar behaviour as reported by Gibb and Long[46]. We can see in Fig. 4.7 that the extrapolation of C_s-ln(ω) curves at different biases meet at a specific point on the frequency axis. As discussed in section 4.1 the frequency corresponding to this point of intersection on frequency axis gives us the magnitude of the upper limit for frequency below

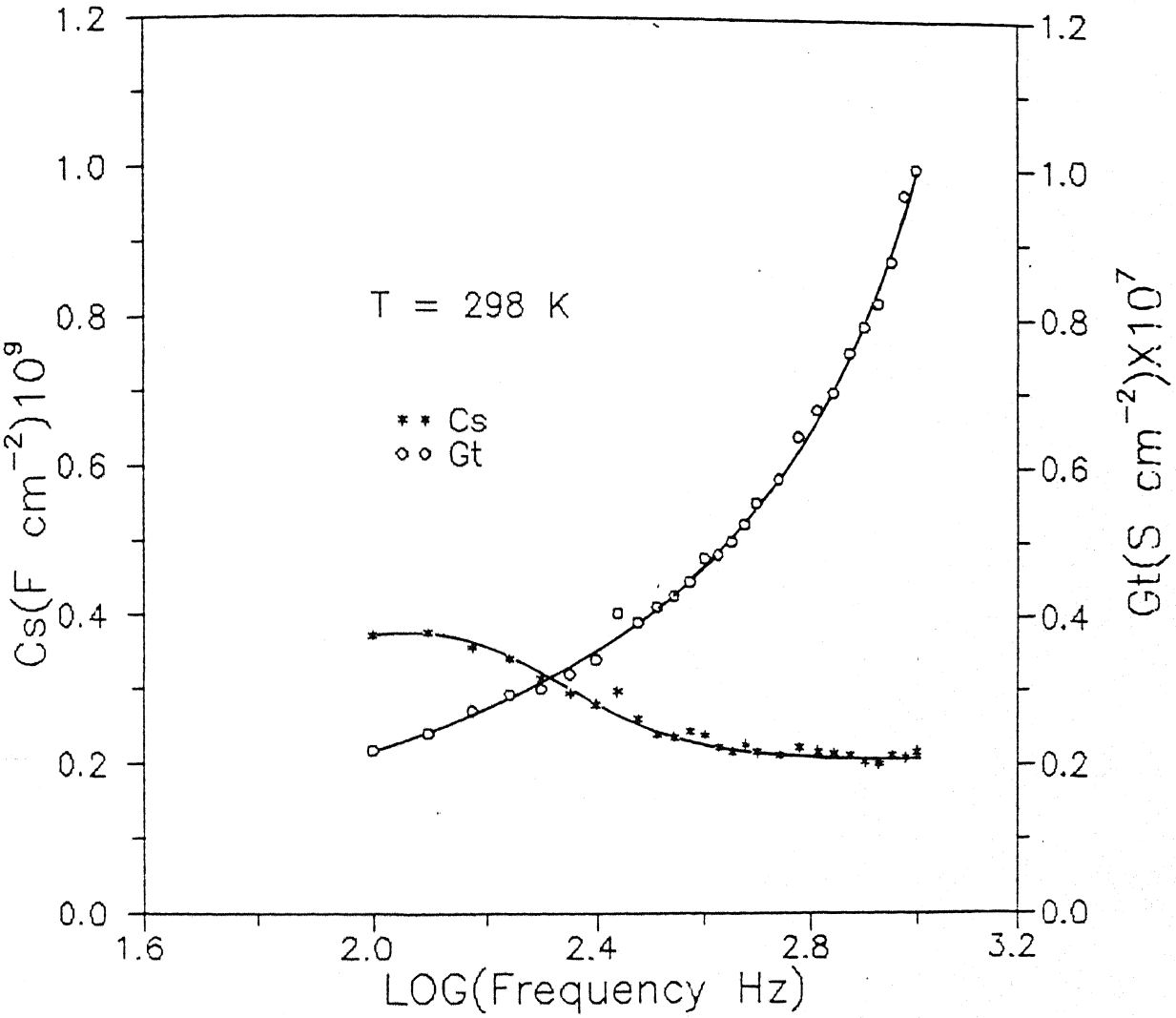

Fig. 4.7. Corrected barrier capacitance (C_s) and conductance (G_s) versus frequency plot at zero dc bias.

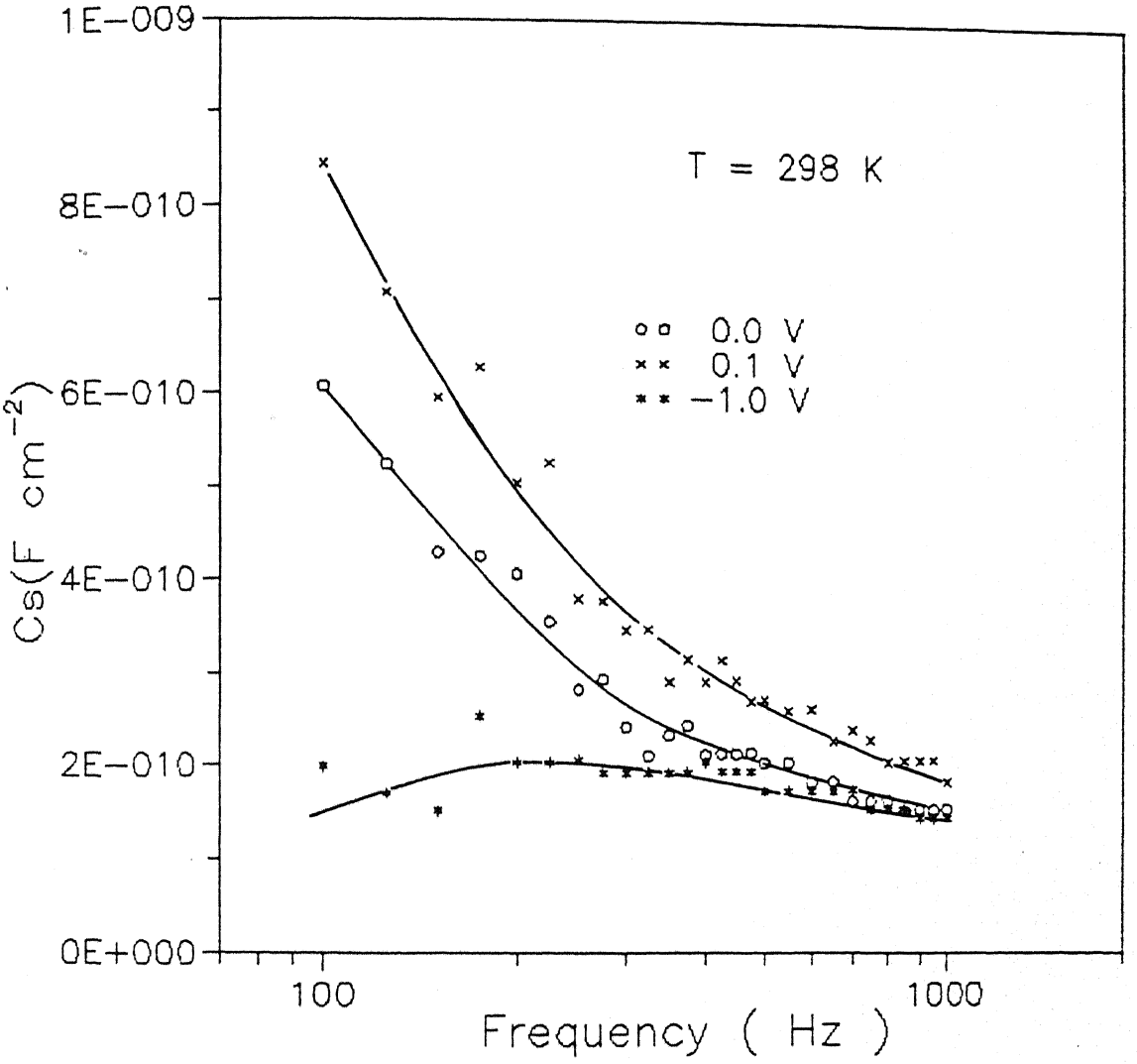

Fig. 4.8. Influence of external dc bias voltage on corrected barrier capacitance versus frequency plots (both forward and reverse).

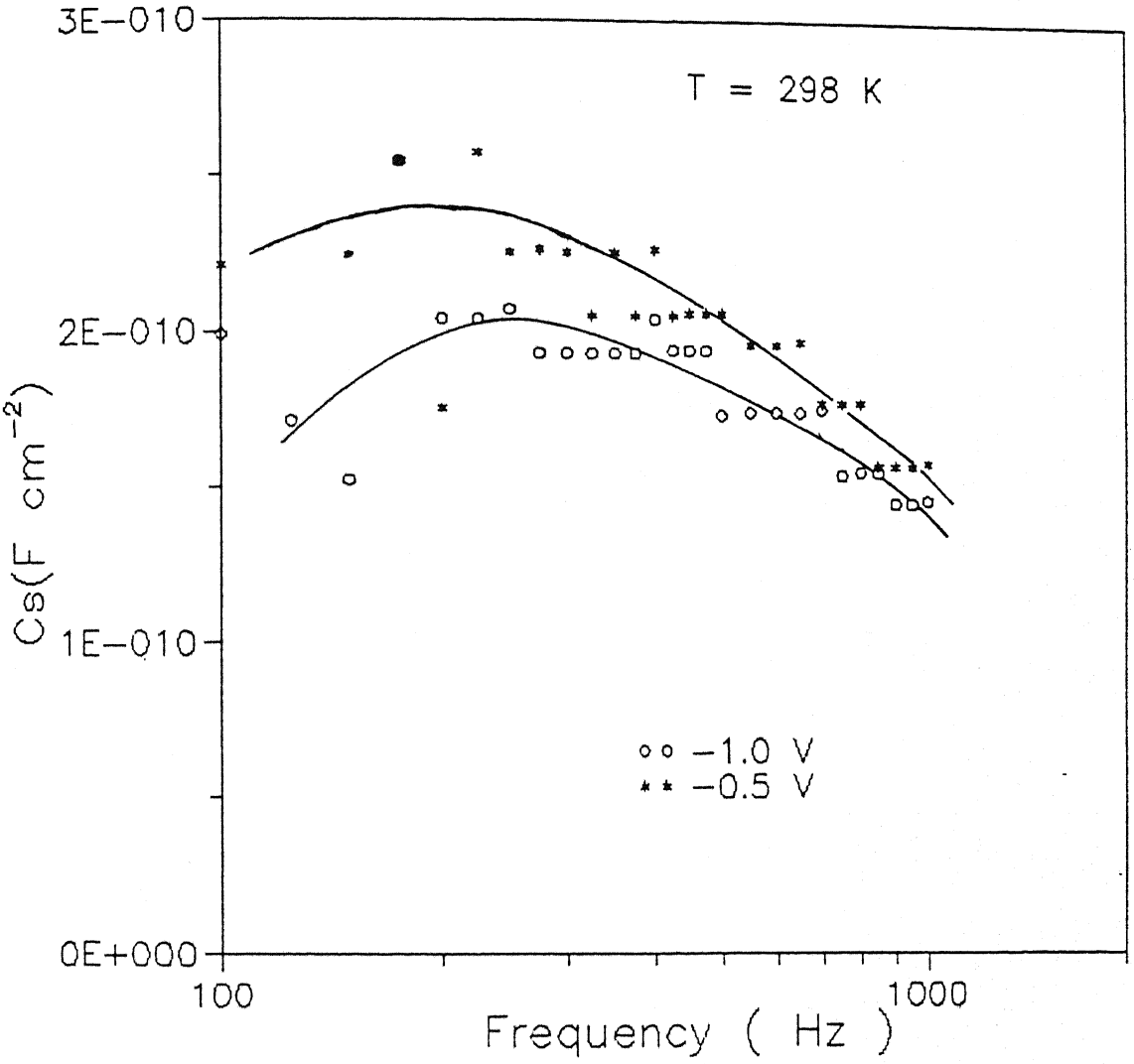

Fig. 4.9. Influence of external dc bias voltage on corrected barrier capacitance versus frequency plots (reverse bias).

which the equivalent circuit cited in Fig. 4.4 is valid. The value of this limiting frequency varies from $2X10^{3}sec^{-1}$ to $2.25X10^{4}sec^{-1}$. So we can write $\tau_0'(=1/\omega) = 1 \pm 5X10^{-4}$ sec. With this τ_0' as on of the parameters, C_0 and V_s are derived from the equations (4.7) and (4.8); the results of this calculation are summarized in Table 4.1. Depending on the choice of initial value of V_s, the value of C_0 varies in the order of its magnitude. Hence we take V_s obtained from the forward bias $1/C_s^2$ vs V plot as a first approximation value for further iterations. The results are discussed below.

To calculate activation energy of the bulk, we can now use the relation $\tau = \tau_0 exp[(E_c - E_F)/kT)$. The empirical parameter τ_0 had been reported to be $(3\pm1)X10^{-14}$ sec by Gibb *et al*[46]. If we use this value of τ_0 then the value of activation energy $(E_a=E_c-E_F)$ appears as (5.9±0.1)eV, which is in good agreement with the value obtained from I-V measurements on the same Schottky diode. The magnitude of V_s derived from this theory is ≈ 0.30 ± 0.05 eV. Therefore the Schottky height, ϕ_b, estimated from the ac measurement becomes

$$\begin{aligned}\phi_b &= (E_c-E_F) + qV_s \\ &\approx (0.59 \pm 0.01) + (0.30 \pm 0.05)\ eV \\ &\approx (0.89 \pm 0.05)\ eV.\end{aligned}$$

We can now recall the dc results listed in Table 3.2. ϕ_b so

obtained from ac mesurements equals that obtained from simulation technique using diffusion theory. So ac results alongwith IPE favour diffusion limited transport and green-signals our model for computer simulation too. Therefore, dc and ac agree well with respect to the diode parametric values of ϕ_b and E_a.

Although our motivation is not to measure DOS in the gap as a function of energy, this model for ac response can easily be extended to estimate it as an indicator of the quality of the material. But with the assumption that DOS in the gap is constant w.r.t. both energy and space. The value of C_o derived from equations (4.7) and (4.8) is replaced from equation (4.10) and then the results so obtained are used in equation(4.4) to calculate the density of states (DOS) in the gap near Fermi energy (N_F) at different applied biases. N_F thus obtanied is $(4\pm4)X10^{-15}$ $cm^{-3}eV^{-1}$ over the bias range 0.2 - 0.3 eV and frequency range 200 - 500 Hz. This value of N_F agrees quite well with the value given in section 2.1, and implies a good quality a-Si:H material.

To summarize the results obtained from ac response of our sample we can mention the following points:

1. predominant features in capacitive behaviour are successfully described in the light of Gibb and Long model[46].

2. Schottky barrier height, ϕ_b, obtained from ac response agrees quite well with that obtained from our simulation technique and IPE measurements as well.

3. Low activation energy than that expected is due to the shift of quasi Fermi level on applying dc bias voltage. Low density of states in the gap is consistent with the large shift in quasi Fermi level on applying dc bias voltage

CHAPTER V

CONCLUSIONS AND SUGGESTIONS FOR FUTURE WORK

We have conducted three different types of measurements on the same Schottky diode formed by thermal evaporation of metal (Au) on etched and polished surface of undoped a-Si:H. These are dark and photo I-V characteristics, internal photoemission measurements, and ac response (capacitive and ac conductive behaviour). On the basis of these studies, which has been the subject matter of Chapters III and IV, we now state the following as conclusions:

1. Good Au Schottky diodes on undoped a-Si:H were obtained, having low ideality factor, n ($\leq$ 1.1), and high rectification ratio ($> 10^5$ at 2.0 V) in the temperature range from 269 K to 417 K.

2. The saturation current, I_s, obtained from the dark I-V measurements under forward bias is not adequate to characterize Schottky barrier parameter. Because saturation current, I_s, includes the effect of bulk resistance and leakage currents, and thereby decreases the Schottky barrier height (ϕ_b = 0.76 eV for TET and = 0.82 eV for DT).

3. A simple computer simulation technique, taking leakage currents and bulk series resistance into account, has been used to get more accurate value of ϕ_b (= 0.82 eV for TET and = 0.89 eV for DT). From the deduced bulk resistance as a function of

temperature, this technique also give the bulk activation energy E_a = (0.53 eV) as energy separation between conduction band edge and quasi Fermi level for electrons. The actual value of E_a will be obtained by adding the shift of quasi Fermi level relative to neutral bulk Fermi level.

4. It is interesting to note that the saturation currents obtained both from the measured dark I-V characteristics and simulation technique using our model, fit equally well to both thermionic emission theory (TET) and diffusion theory (DT). This makes both theories equally probable, so it is difficult to distinguish between the thermionic emission theory and the diffusion theory. Therefore, I-V characteristics alone (neither direct measured nor computed I-V characteristics) cannot in any way, help us to identify the predominant carrier transport mechanism over the Schottky barrier on a-Si:H.

5. However, it can be done using the results of our model and simulations along with the results of IPE, and then comparing them. We have found that the ϕ_b (= 0.92±0.02 eV) obtained from IPE measurements agree well, within experimental error, with that (=0.89 eV)obtained from our simple model for computer simulation, using diffusion theory. Since the actual transport mechanism should result in correct value of ϕ_b (as obtained from IPE), diffusion limited transport is the most likely mechanism in a-Si:H Schottky diodes.

6. The dominant features of capacitive and conductive behaviours, measured as a function of both frequency and bias on this diode, are successfully interpreted using a straight-forward Gibb-Long model[46]. A simple simulation along with this model results in reasonable activation energy (E_a= 0.59 eV), diffusion voltage (V_d= 0.3 ± 0.05 eV) Schottky barrier height (ϕ_b= 0.89 ± 0.05 ev).

7. Schottky barrier height obtained from ac response agrees quite well with that obtained from our simulation technique and IPE measurements as well. In fact, this provides another support to diffusion theory and the simulation process as well.

8. Low activation energy than expected is due to the shift of quasi Fermi level on applying dc bias voltage. Low density of states in the gap is consistent with the large shift (0.23 eV) in quasi Fermi level on applying dc bias voltage (1.0 V)

9. We conclude that the functional dependence of series resistance R_s on applied bias voltage is responsible for the deviation, specially at higher biases, of computed I-V characteristics from measured one. It is necessary to find it nature of functional dependence on bias to obtain better fitting. This will also improve the value of saturation currents and hence the Schottky barrier height more close to that of IPE. Our model and simulation technique, in any case, offer better results. We can , therefore, recommend this process to obtain good results and

more reliable information than that obtained from commonly used simple I-V characteristics as a function of temperature.

SUGGESTIONS FOR FURTHER WORK:

The line of investigations pursued in this work can be extended for Schottky barriers with metals other than gold. The characteristics of Schottky barrier diodes on a-Si:H is very sensitive to the surface conditions and even degrades on storage. This aspect can be studied systematically using techniques and analyses as employed here. Capacitance measurements should be extended to temperatures other than room temperature.

LIST OF REFERENCES

1. F. Braun, Pogg. Ann., 153, 553, (1874)
2. Mott and devis, *Eectronic Processes in Non-crystalline Materials*, second edition (Clarendon press, Oxford, 1979)
3. P. G. Lecomber, J. Non-cryst. Solids, 115, 1, (1989)
4. D. E. Carlson, J. Non-cryst. Solids, 35/36, 707, (1980)
5. C. R. Wronski, D. E. Carlson, and R. E. Daniel, Appl. Phys. Lett., 37, 96, (1976)
6. J. Pankove, *Semiconductos and semimetals*, vol. 21, Part C (Academic Press, London, 1984)
7. S. M. Sze, *Physics of Semiconductor Devices, Second edition* (J. Wiley and Sons, New York)
8. M. J. Thompson, N. M. Johnson, R. J. Nemanich, and C. C. Tsai, Appl. Phys. Lett., 39, 274 (1981)
9. R.J. Nemanich, C. C. Tsai, M. J. Thompson, and T. W. Sigmon, J. Vac. Sci. Technol., 19, 685, (1981)
10. R. J. Nemanich, M. J. Thompson, W. B. Jackson, C. C. Tsai , and B. L. Stafford, J. Vac. Sci. Technol., B 1, 519 (1983)
11. R. J. Nemanich and C. M. Doland, J. Vac. Sci. Technol., B 3, 1142 (1985)
12. B. L. Sharma, *Schottky Barrier Junctions and Thei Applications* (Plenum Press, New York, 1984)
13. D. V. Lang, J. D. Cohen, and J. P. Harbison, Phys. Rev. B 25, 6285 (1982)
14. W. B. Jackson and N. M Amer, Phys. Rev.,B 25, 5559 (1982)
15. W. B. Jackson and N. M. Amer, and R. J. Nemanich, Phys. Rev., B 29 4861 (1983)
16. E. H. Rhoderick, *Metal-Semiconductor Contacts* (Clarendon press, Oxford, 1978)
17. V. Heine, Phys. Rev. A 138, 1689 (1965)
18. J. Tersoff, Phys Rev. Lett., 52, 465 (1983)
19. W. E. Spicer, I. Lindau, P. R. Skeath, C. Y. Su, and P. W. Chye, Phys. Rev. Lett., 44, 420 (1980)
20. R. E. Allen and J. D. Dow, Phys. Rev., B 25, 1423 (1982)
21. J. Y. Duboz, Phys. Rev., B 40, 10607 (1989)
22. R. Ludeke, G. Jezequel, and A. Taleb-Ibrahimi, Phys. Rev. Lett., 4, 91 (1964)

23. K. Stiles, and A. Kahn, Phys. Rev. Lett., 60, 440 (1988)

24. R. M. Feenstra and P. Martnsson, Phys. Rev. Lett., 61, 447 (1988)

25. R. J. Haustein, T. E. Schlezinger, T. C. McGill, B. D. Hunt, and L. J. Schowalter, Appl. Phys. Lett., 47, 853 (1985)

26. C. R. Wronski and D. E. Carlson, Solid State Commun., 23, 421 (1976)

27. M. J. Thompson, M. M. Alkaisi, and J. Allison, IEEE. Proc. 127, 212 (1980)

28. A. J. Snell, K. D. Mackenzie, P. G. LeComber, and W. E. Spear, Phill. Mag., B 40, 1 (1979)

29. Y. Michima, M. Hirose, and Y. Osaka, Jpn. J. Appl. Phys. 20, 593 (1981)

30. D. Jousse, P. Vikatorovitch, L. Vieux-Rochaz, and A. Chenevas-Paule, J. Non-cryst. Solids, 36, 767 (1980)

31. M. M. Akaisi and M. J. Thompson, Solar Cells, 1, 91 (1979- 1980)

32. M. Hicks, S. Lee, S. Kumar, C. R. Wronski, and M. Pinarbasi, Mat. Res. Soc. Symp. Proc. 149, 303, (1989)

33. A. A. Pasa etal 137/138 ,1087 (1991)

34. C. R. Wronski, B. Abeles, T. Tiedje, and G. D. Cody, Solar Cells, 2, 245 (1980)

35. S. Lee, S. Kumar, C. R. Wronski, and N. Maley, J. Non-cryst. Solids, 114, 316 (1989)

36. I. Chen and S. J. Lee, J. Appl. Phys., 53, 1045 (1982)

37. J. L. Freeouf, T.N. Jackson, S. E. Laux, and J.M.Woodall J. Vac. Sci. technol., 21, 570 (1982)

38. C. R. Wronski, Jpn. J. Appl. Phys., 17, 299 (1978)

39. A. Deneuville and M. H. Brodsky, J. Appl. Phys.,50 1414 (1979)

40. D. Donoval, J. De Sousa Pires, P. A. Tove, a Solid State Elec., 32, 969 (1989)

41. C. R. Wronski, B. Abeles, G. D. Cody, and T. Tiedj Appl. Phys. Lett., 37, 96 (1980)

42. R. J. Nemanich, M. J. Thompson, W. B. Jackson, C.C. Tsai, and B. L. Staffod, J. Non-Cryst. Solids, 59/60, 513 (1983)

43. T. Yamoto, Y. Mishima, M. Hisore, and Y. Osaka, Jpn. J. Appl. Phys. , 20 suppl. 20-2, 185 (1981)

44. C. R. Wronski, S. Lee, M. Hicks, and Satyendra Kumar, Phys. Rev. Lett., 63, 1420 (1989)

45. W. Den Bôer, J. Phys., Paris, 42, C4-451 (1981)

46. I. G. Gibb and A. R. Long, Phill. Mag. B, 49, 565 (1984)

47. A. Madan, W. Czubatyj, J. Young, M. S. Shur, and M. P. Shaw, Appl. Phys. Lett., 40, 234 (1982)

48. W. E. Spear, P. G. Le Comber, and A. J. Snell, Phill. Mag. B, 38, 303, (1978)

49. J. Beichler, W. Fuhs, H. Mell, and H. M. Welsch, J. Non-Cryst. solids, 35/36, 587 (1980)

50. P. Viktorovitch, and G. Moddel, J. Appl. Phys., 51, 4847 (1980)

51. A. J. Snell, and Mackenzie, Phill. Mag. B, 40, 1 (1979)

52. Fernandeze Canque et al , J. Appl. Phys., 54, 7025 (1983)